Laboratório de
Implantação Iônica

Instituto de Física - UFRGS

Years

Annual Report 2012

Laboratório de
Implantação Iônica
Instituto de Física - UFRGS

Annual Report 2012

Editors

Daniel Lorscheitter Baptista

Raquel Giullian

Pedro Luis Grande

Table of contents

Preface

The Ion Implantation Laboratory is an ion beam center at the Institute of Physics (IF) at the Federal University of Rio Grande do Sul (UFRGS), Brazil. The IF-UFRGS is located in the city of Porto Alegre (state of Rio Grande do Sul) and it is ranked as the most important research center of Physics in southern Brazil. The staff of the Institute is composed of 83 Ph.D. researchers divided in two Departments (Physics and Astronomy). Currently, the Institute has around 120 graduate students and is responsible for the Physics courses to approximately 2000 undergraduates of different fields.

The activities on ion beams started in 1981 with the acquisition of a 400 kV particle accelerator (which was modified to 500 kV in 1996). In 1989 an ion implanter of 250 kV was donated by IBM (USA) and is currently dedicated to microelectronic applications. In January 1995 an important upgrade was done with the acquisition of a 3 MV TANDEM accelerator. Both machines provide a wide variety of positive ions in a broad energy range. Several beam lines with different analytical techniques are available to scientists from different fields. The techniques are:

1) **PIXE** (Particle-Induced X-ray Emission): provides elemental concentrations of the order of part per million;
2) **RBS** (Rutherford Backscattering Spectrometry): used for characterization of different structures, including multi-layered targets;
3) **NRA** (Nuclear Reaction Analysis) and **NRP** (Nuclear Reaction Profiling): ideal to detect and profile specific isotopes respectively;
4) **Microprobe**: allow the use of techniques like PIXE, RBS and STIM with micrometer beam size;
5) **MEIS** (Medium Energy Ion Scattering): it is a high-resolution RBS technique with isotope-separation capability;
6) **Ion Implantation**: used for modification of materials under controlled parameters.

The infrastructure of the laboratory includes a large variety of charged-particle, X-ray and gamma detectors, modular electronics, ovens and other related equipment. A fully-dedicated workshop allows the maintenance of the laboratory in a regular basis. A general view of the laboratory is shown below, featuring the beam lines of the Tandetron accelerator.

In the Ion Implantation Laboratory were also developed many software used worldwide for characterization of nano-structures (PowerMeis - program), electronic stopping power (CasP-program) among others developed for nuclear reaction profiling and MEIS (Flatus – program) and for data acquisition (Feiticeira, MEIX).

Many researchers from the Ion Implantation Laboratory are also engaged to other labs or facilities from IF-UFRGS. In particular the Laboratory of Microelectronics and the Laboratory of Solid Interfaces and Surfaces are associated laboratories and share many scientific projects.

This is the third issue of the annual report and we are celebrating the 30th foundation anniversary of the Ion Implantation Laboratory. Since our first beam time on 7th October 1982, an implantation of 100 keV N ions, lots of things have happened. International conferences have been organized, many students got graduated (about 60 P.h.Ds) and about 1000 scientific articles have been published so far. And of course, for all these reasons and others, the Ion Implantation Laboratory is part of the life of hundreds of people. The Lab. founded by Prof. Zawislak in the 80s has grown a lot considering all indicators (people, facilities and science) and now is a patrimony of our university. It is our responsibility to preserve it and to go further.

Pedro L. Grande
Head of Ion Implantation Laboratory

30 years implanting ideas

The Ion Implantation Laboratory has its history starting in 1981, however the process of establishing the research plan that led to the decision of the acquisition of this equipment started many years before that. Since its set up it became a nucleation of changes, starting with the change of the role institute to a new campus that would have space for the implementation of the project.

Over the years, this laboratory was responsible for forming professionals in different areas of material science. Similarly to other large laboratories it plays an important role as focal point where researchers work together and share new ideas. At the educational level it represents an opportunity for young researchers and students to learn how physics can advance faster due to cooperative work.

Realizing that advances in science can not be tide to machines, but that machines are instruments of discoveries, the laboratory had expanded the machine to more energetic beams with the acquisition of the Tandem accelerator and had implemented new techniques such as PIXE, RBS, NRA, Microprobe and MEIS.

Over the years, a number of research groups had utilize the laboratory and many others had been created as the result of the melting pot of ideas that are generated by this large gathering of scientists.

The Ion Implantation Laboratory has proved to be an important place for advances of science, for the nucleation of fields and researchers and as an school for educating the new leading researchers in Brazil.

Marcia Barbosa
Director

Instituto de Física
Universidade Federal do Rio Grande do Sul

First ion implantation

The document below describes the first ion implantation performed at the Ion Implantation Laboratory in October 7th, 1982. It was used a 100 keV N_2^+ beam with current density of 1.5 mA.cm^{-2}. The document is handwritten and assigned by the lab. founder Prof. Fernando Zawislak. The experiment was followed by the other staff members Joel P. de Souza, Moni Behar, Rogério Livi, Clodomiro Castello and Celso Müller.

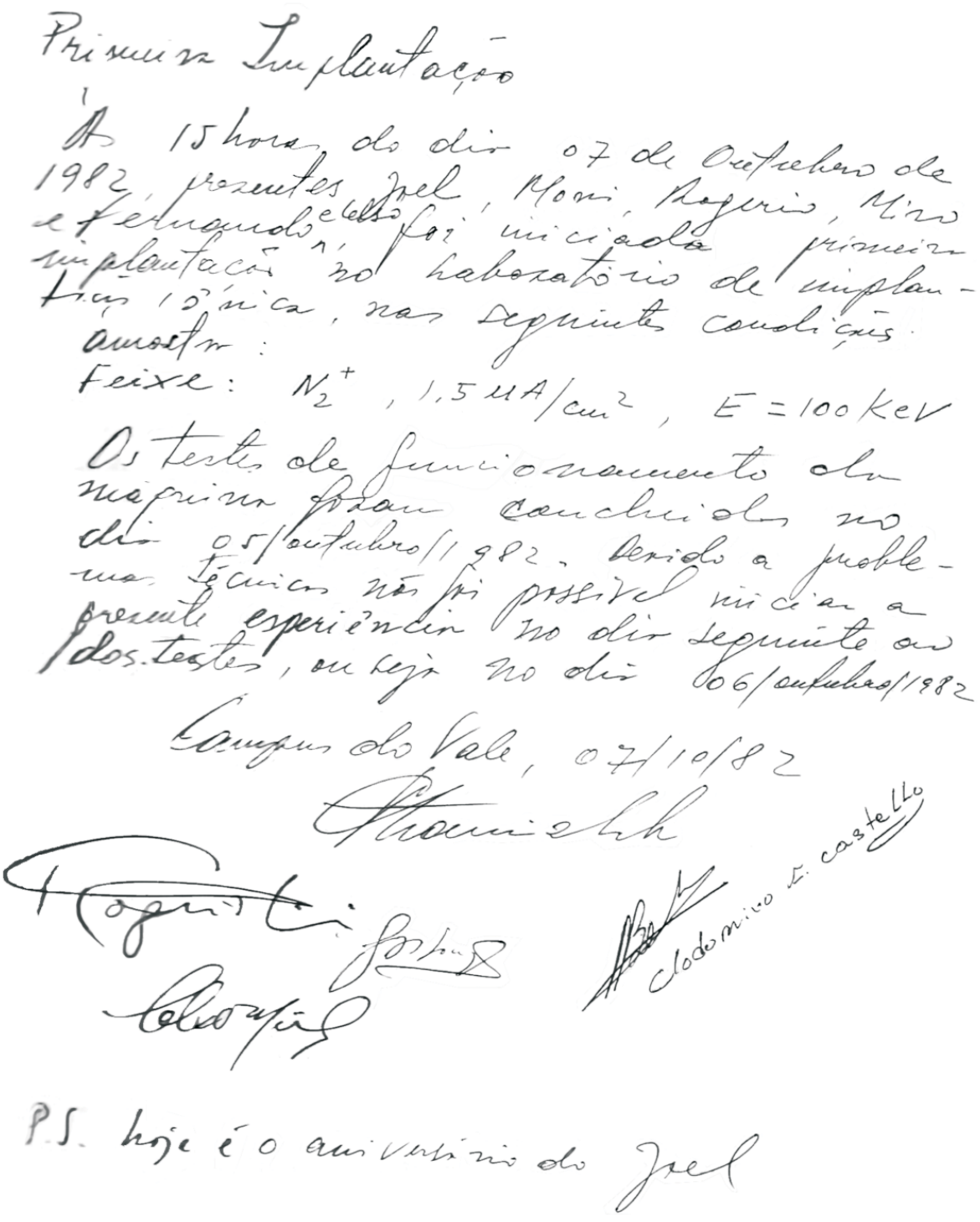

Primeira Implantação

Às 15 horas do dia 07 de Outubro de 1982, presentes Joel, Moni, Rogério, Nivo e Fernando Zawislak foi iniciada a primeira implantação no laboratório de implantação iônica, nas seguintes condições:

amostra:

feixe: N_2^+, 1,5 μA/cm², E = 100 keV

Os testes de funcionamento da máquina foram concluídos no dia 05/outubro/1982. Devido a problemas técnicos não foi possível iniciar a presente experiência no dia seguinte ao dos testes, ou seja no dia 06/outubro/1982

Campus do Vale, 07/10/82

Fernando Zawislak

Rogério Livi

Joel P. de Souza

Clodomiro C. Castello

Celso Müller

P.S. hoje é o aniversário do Joel

Staff - 2012

Permanent

Fernando Claudio Zawislak, PhD. (IF, UFRGS, 1967) - Founder and Group leader between 1980 and 2008

Moni Behar, PhD. (UBA, ARGENTINA, 1970) – Accelerators coordinator between 1982 and 2009

Israel Jacob Rabin Baumvol, PhD. (IF, UFRGS, 1977)

Livio Amaral, PhD. (IF, UFRGS, 1982)

Paulo Fernando Papaleo Fichtner, PhD. (IF, UFRGS, 1987)

Pedro Luís Grande, PhD. (IF, UFRGS, 1989) - Group leader since 2009.

Johnny Ferraz Dias, PhD. (UG, BELGIUM, 1994) – Accelerators coordinator since 2010.

Henri Ivanov Boudinov , PhD. (IE-BAN, BULGARY, 1991)

Fernanda Chiarello Stedile, PhD. (IQ, UFRGS, 1994)

Ricardo Meurer Papaléo, PhD. (U.UPPSALA, SWEDEN, 1996) - PUC-RS

Rogério Luis Maltez, PhD. (IF, UFRGS, 1997)

Claudio Radtke,PhD. (IF, UFRGS, 2003)

Cristiano Krug, PhD. (IF, UFRGS, 2003)

Gustavo de Medeiros Azevedo, PhD. (IF, UFRGS, 2000)

Daniel Lorscheitter Baptista, PhD. (IF, UFRGS, 2003)

Gabriel Viera Soares, PhD. (IF, UFRGS, 2008)

Raul Carlos Fadanelli Filho, PhD. (IF, UFRGS, 2005)

Rafael Peretti Pezzi, PhD. (IF, UFRGS, 2009)

Leandro Langie Araujo, PhD. (IF, UFRGS, 2004)

Raquel Giulian, PhD. (RSPE, ANU, AUSTRALIA, 2009)

Agenor Hentz da Silva Jr., PhD. (IF, UFRGS, 2007)

Technicians

Agostinho A. Bulla, Electrical Engineer responsible for the accelerators

Zacarias E. Fabrim, Mechanical Engineer responsible for the clean-room

Clodomiro F. Castello, Accelerator support and operation

Paulo R. Borba, Accelerator support and operation

Michele Richter , Accelerator support and operation

Paulo Kovalik, Workshop

Éder Bidinotto Brito, Sample preparation and cleanroom assistant

Postdocs

Carla Eliete Iochims dos Santos

Flavia Piegas Luce

Maria Lúcia Yoneama

Paulo Fernandes Costa Jobim

Paulo Licenio Franzen

Silvina Limardi

Wellington Fernandez

PhD Students

Anaí Duarte

Augusto A. D. de Mattos

Caroline Lisevski

Cláudia Telles de Souza

Cristiane Marin

Dario F. Sanchez

Deise Schafer

Eliasibe Luis de Souza

Elis Moura Stori

PhD Students (continued)

Felipe Bregolin

Guilherme Sombrio

João Wagner Lopes de Oliveira

Josiane Bueno Salazar

Liana Appel Boufleur

Lucio Rosa

Ludmar Guedes Matos

Luiz Acauan

Maurício Sortica

Nicolau Molina Bom

Rafael Otoniel

Rafaela Debastiani

Ramon Ferreira Jr.

Roberto Moreno de Souza Reis

Silma Alberton Corrêa

Tiago Silva de Avila

Zacarias Eduardo Fabrim

MSc students

André L. F. Cauduro

Antônio Eudocio Pozo de Mattos

Eder Sandim Ximenes

Eduardo Pitthan Filho

Gabriel Marmitt

Guilherme Rolim

Ivan Rodrigo Kaufmann

Luiza Raquel Manfredi da Silva

Masahiro Hatori

Matheus Adam

Rafael J. Pauliello

International collaborators

L. Thome, Orsay, France.

F. Garrido, Orsay, France.

W. Skorupa Rossendorf, Germany.

L. Rebohle, Rossendeorf, Germany.

I. Abril, University of Alicant, Spain.

F. Garcia- Molina University of Murcia, Spain.

G. Garcia Bermudez, Lab. Tandar CNEA, Argentina.

N. Arista CAB, CNEA, Argentina.

S. Suarez CAB, CNEA, Argentina.

G. Lucovsky, NCSU, USA.

J.M.J. Lopes, PDI, Germany.

L. Feldman, Rutgers University, USA.

A. Agarwal,Cree Inc., USA.

A. Lelis, Army Research Lab., USA.

S. Dimitrijev, Griffith University, Australia.

G. Schiwietz, Helmholtz-Zentrum Berlin, Germany.

J. Kennedy, GNS, New Zealand.

H. Rothard, GANIL, France.

International collaborators (continued)

C. D. Denton, University of Alicant, Spain

D. K. Ferry, Arizona State University, USA.

V. Mittin, State University of New York at Buffalo, USA.

M.C. Ridgway, The Australian National University, Australia.

H.G. Rubahn, NanoSYD, Sonderborg, Denmark.

Z. Liliental-Weber, LBNL, USA.

C. Trautmann, GSI, Darmstadt, Germany.

F. Aumayr,Vienna University of Technology, Vienna, Austria

E. Oliviero, University of Paris-Sud (Orsay), France.

J-F Barbot, University of Poitiers, France.

M. F. Beaufort,University of Poitiers, France.

S. Reboh, Laboratoire d'électronique des technologies de l'information, Grenoble, France.

Brazilian collaborators

L.M. Nagamine, USP, São Paulo
R.P. Menezes, PUC, Rio de Janeiro
E.F. da Silveira, PUC, Rio de Janeiro
L.S. Farenzena, UFSC, Florianópolis
G. Machado, CETENE, Recife
L. Miotti, Caxias do Sul
J. Geshev, UFRGS, Porto Alegre
L.G. Pereira, UFRGS, Porto Alegre
M. Schiavon, UFSJ, São João del-Rei
U.S. Sias, IFSul-Campus Pelotas
E.F. da Silva Jr., UFPE, Recife
A.A. Pasa, UFSC, Florianópolis
I. Hummelgen, UFPR, Curitiba
J.W. Swart, CTI, Campinas
J.A. Diniz, UNICAMP, Campinas
G. Kellermann, UFPR, Curitiba
A. Malachias, UFMG, Belo Horizonte
T. Marcondes, CBPF, Rio de Janeiro
R.L. Sommer, CBPF, Rio de Janeiro
L. Sampaio, CBPF, Rio de Janeiro
V.P. Mammana, CTI, Campinas
L. F. Schelp, UFSM, Santa Maria
M. Carara, UFSM, Santa Maria
L. S. Dorneles, UFSM, Santa Maria
V. Moraes, UNESC, Criciúma
S. Francke, UNISC, Santa Cruz do Sul
J. Silva, ULBRA, Canoas
D. Mosca, UFPR, Curitiba

Facilities

Besides the accelerators the laboratory has the following facilities:

a) Photoluminesce laboratory

b) Cleanroom

c) Furnaces, ovens and reactor chambers

d) Scanning electron microscope

Tandetron accelerator

500 kV accelerator

250 kV accelerator

Furnaces and reactors

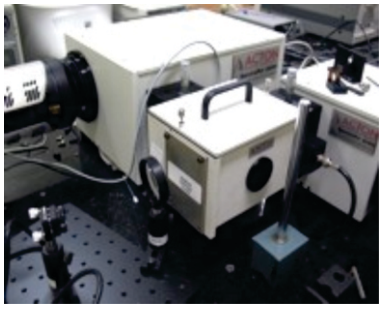

Optical characterization

Cleanroom

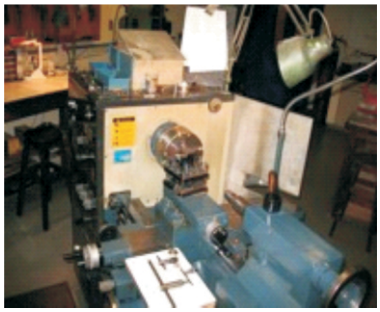

Workshop

Support room

Scanning electron microscope

Research Projects

Structural characterization of CdSe/ZnS quantum dots through medium energy ion scattering

M. A. Sortica, P. L. Grande, C. Radtke, L. Almeida, R. Dabastiani, J. F. Dias, A. Hentz

Introduction

In this work, we have used medium energy ions scattering (MEIS) together with transmission electronic microscopy (TEM), Rutherford backscattering spectrometry (RBS) and particle induced X-ray emission (PIXE), to characterize CdSe/ZnS core-shell quantum dots. The overall elemental fractions were determined by RBS and PIXE, and the internal structure was analyzed by MEIS. For this sake, we have used our Monte Carlo software, called PowerMeis, to simulate the full 2D MEIS spectra from different structural models.

Results

We observed that, although the sample having a ratio Cd:Se of 0.69:0.31, the core is a stoichiometric CdSe crystal and the excess of cadmium are distributed over the shell, forming a structure CdSe/CdZnS. The diameter obtained for the core, of 5.2 nm, is in agreement with the TEM images and the photoluminescence spectrum of the nanocrystals.

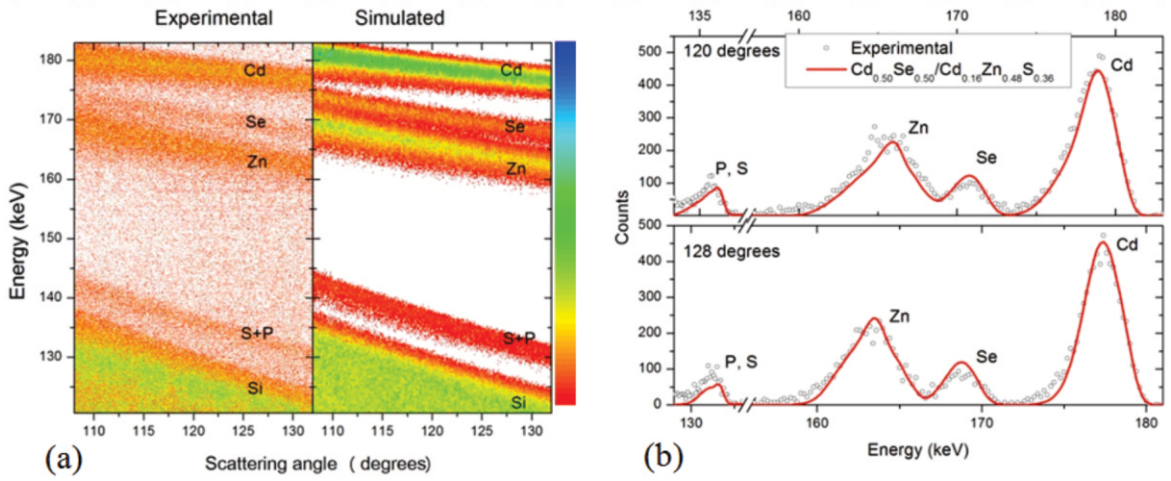

Figure 1 *(a) MEIS spectra, experimental and simulated, of the quantum dots core-shell CdSe/ZnS deposited on silicon (1 0 0). (b) Best fit of MEIS spectrum, taking into account different structural models, measured at two scattering angles.*

Research Outlook

This study shows that the MEIS technique, combined with other analytical techniques, is a powerful tool to determine elemental distribution profiles within nanoparticles, with diameter approximately 5 nm, which can hardly be obtained by other techniques. This allows studies of the formation and stability of the internal structure of the QDs when exposed to various types of processes such as heating and irradiation of ions.

Publications

[1] M. A. Sortica, P. L. Grande, C. Radtke, L. Almeida, R. Debastiani, J. F. Dias, A. Hentz, *Structural characterization of CdSe/ZnS quantum dots using medium energy ion scattering*, Applied Physics Letters, **101**, 023110 (2012)

MEIS, TEM and XPS analysis of iron-based core/shell nanostructures

D. F. Sanchez

Introduction

Understanding the properties of nanomaterials requires understanding the structure, composition, and chemistry. However, to date, there is no single method that can provide quantitative information about these three properties. Medium energy ion scattering (MEIS) is an ion beam characterization technique capable to determine with subnanometric depth resolution distributions of different elements in a single nanoparticle (NP) and, also, sensitive to characterization of shape, composition, size distribution and stoichiometry NP systems. Using the PowerMeis simulation and fitting software, that considers any geometry, size distribution, composition and density of the nanostructures, here we shown the capability of MEIS analysis combined with energy-resolved X-ray photoelectron spectroscopy (XPS) and Transmission Electron Microscopy (TEM) to characterize a near the surface iron based core/shell NPs system embedded in SiO_2 [1].

Results

The samples were synthesized through low energy ion beam implantation followed by 60 s of electron beam annealing [2]. The NPs geometrical features, such as geometrical parameters, size distribution and correlation were characterized through TEM analysis. The core was identified as crystalline Fe. The shell stoichiometry was obtained (between $Fe_{14}Si_{19}O_{67}$ and $Fe_{16}Si_{22}O_{61}$) by constraining the MEIS analysis with parameters extracted from TEM observations. Also, the depth profiles of the relative amounts of Fe in the core and in the shell from MEIS-TEM analysis and the relative amounts of metal Fe^0 and Fe^{2+} from energy-resolved XPS measurements were compared, obtaining an excellent agreement between each other.

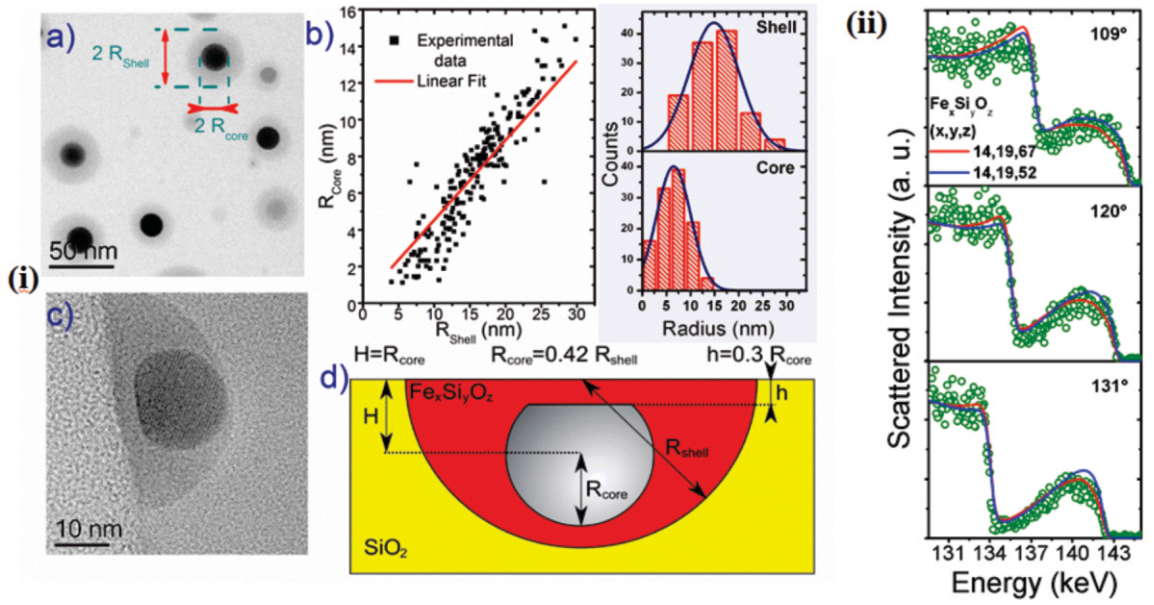

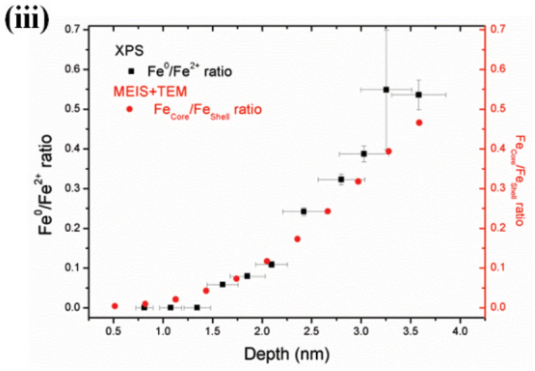

Figure 1 - *(i) Through TEM observations from (a) plan-view and (c) cross-sectional samples, the size distribution and shape (b) were obtained and used to (d) model the NPs. (ii) These features were taken into account in the MEIS analysis, where the stoichiometry was refined to fit the MEIS data. (iii) Comparison of the depth profiles of the relative amounts of Fe in the core and in the shell from MEIS/TEM analysis and the relative amounts of metal Fe_0 and Fe^{2+} from XPS measurements.*

Research Outlook

TEM and energy-resolved XPS provide local information of nanostructures with subnanometrical resolution. The former one have lateral and depth resolution (tridimensional structure) and the latter offers a chemical/compositional information with depth resolution. The combination of these two techniques with MEIS, demonstrated to be an useful tool and opens up new perspectives for the investigation of buried nanostructures into solid matrices, with interest both in the scientific and technological point of view.

Publications

[1] J. Leveneur, D. F. Sanchez, J. Kennedy, P. L. Grande, G. V. M. Williams, J. B. Metson, B. C. C. Cowie, *Iron-based bimagnetic core/shell nanostructures in SiO_2: a TEM, MEIS, and energy-resolved XPS analysis*, Journal of Nanoparticle Research, **14**, 1149 (2012).
[2] J. Kennedy, J. Leveneur, G. V. M. Williams, D. Mitchell, A. Markwitz, *Fabrication of surface magnetic nanoclusters using low energy ion implantation and electron beam. Nanotechnology*, **22**, 115602 (2011).

In situ observations of migration and coalescence phenomena for Pb nanoparticles embedded in silica films

P. F. P. Fichtner

Introduction

Because of their enormous interface area to volume ratio, nanoparticle (NP) systems are intrinsically in a non-thermodynamic equilibrium state and tend to evolve via coarsening processes driven by the reduction of the total interface free energy. Fundamental knowledge on the coarsening mechanisms and their rates is highly desired because the phenomenon can be considered as a thermodynamic tool in order to tailor the NP system properties by changing their size and number density. In this contribution we report on the thermal stability and microstructure evolution of Pb nanoparticle systems submitted to high temperature (400 to 1100 °C) thermal treatments and in-situ TEM electron irradiation. The samples were prepared by implanting Pb ions into 200 nm thick thermally grown silica films kept at room temperature, following a procedure described elsewhere in previous ex-situ investigations [1]. In comparison with these ex-situ results, in-situ experiments reveal that the combination of high temperature and electron irradiation from the 200 kV beam used in the TEM observations significantly affect the microstructure evolution of the system.

Results

We demonstrate that, at temperatures above 400 °C, the electron beam enhances NP nucleation and atomic Pb redistribution. In addition, at 1100 °C, the electron irradiation induces the migration of liquid Pb NPs embedded in the film, which can reach distances much higher than the particle diameter, thus promoting a migration and coalescence coarsening process. The in-situ TEM thermal treatments and electron irradiation were registered using a high frame-rate CCD camera. A careful video analysis indicates that the NP migration process presents a Brownian-like behavior.

The determination of effective diffusion coefficients from individual particles as a function of their radius suggests that the NP migration process is governed by an electron-irradiation-enhanced interface diffusion of matrix atoms, discussed considering either elastic atomic displacements or adiabatic breakdown of atomic bounds of matrix atoms at the particle interface region [2].

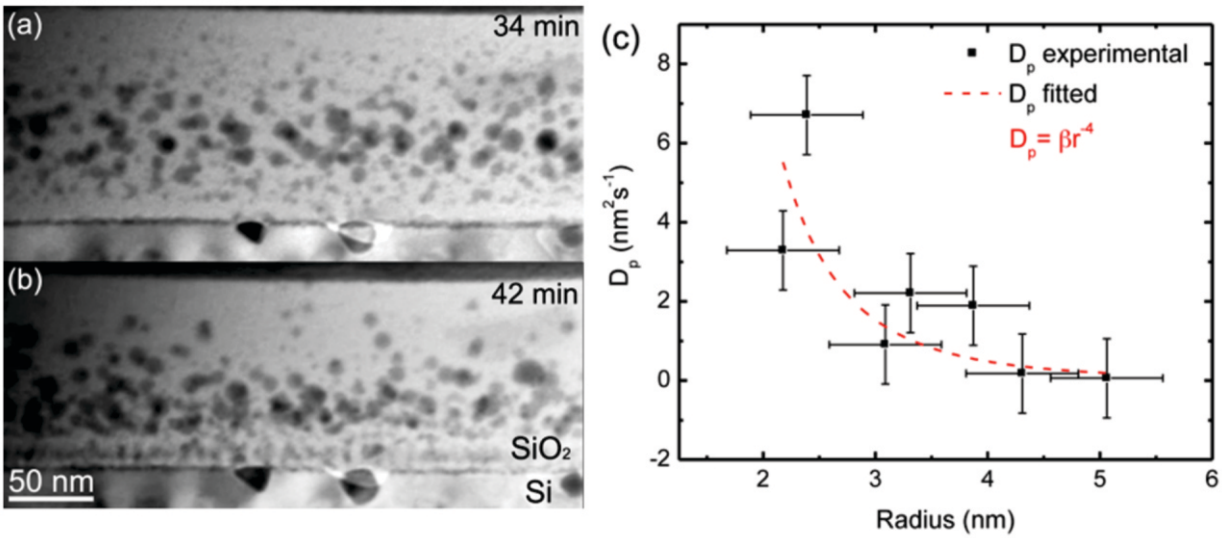

Figure 1 - *Sequence of micrographs from the same sample region obtained during in-situ 1100 ºC TEM thermal annealing after (a) 34 and (b) 42 minutes of high temperature treatment. (c) Particle diffusivity coefficient Dp as a function of NP radius. The data points were experimentally obtained from the video recorded during 1100 ºC in-situ thermal annealing and are consistently fitted by Dp = βr-4 (for β = 124) suggesting that particle growth is governed by migration and coalescence processes mainly controlled by surface diffusion mechanisms.*

Research Outlook

The present experiments introduce a model case system that tackles the stability of nanoparticles, enlightening the effects of energetic particle irradiation-annealing treatments and identifying issues that could hamper their long-term applications in radiation-harsh environments as in space or nuclear sectors.

Publications

[1] F. P. Luce, et al, J. Appl. Phys. **109**, 014320 (2011)
[2] F. P. Luce, PhD Thesis, *Estabilidade de nanopartículas em sílica: efeitos térmicos e de irradiação com elétrons e íons energéticos.* IF-UFRGS 2012

Ion beam modification and thermal stabillity of Pb nanoparticles embedded in silica, observed by in situ TEM

G. Azevedo

Introduction

Nanoparticles (NP's) embedded in dielectric thin films can be obtained by ion implantation followed by high temperature thermal annealing. The control of the size distribution of NP's embedded in dielectrics has been subject of intensive investigations in recent years. It has been suggested that the non-equilibrium conditions during irradiations with energetic ion beams can influence their growth mechanisms. Ion irradiation and annealing temperature operate in opposition. Depending on the irradiation conditions and temperature, the Ostwald Ripening (OR) process can be reverted. Under irradiation, a NP acts as a source, increasing the solute concentration in the surrounding matrix, eventually leading to the formation of an halo of small satellites around the original NP. Analysis of the satellites size distribution and distance from the original nanoparticle yields invaluable information on two main parameters that govern NP formation, i.e., surface energy and atomic diffusion under ion irradiation. This suggests that both parameters can be fine tuned, providing a pathway to the control of NP size distribution.

Results

Herein we report results on the irradiation of Pb nanoparticles embedded in silica submitted to ion irradiation with 4 MeV Au ions at room temperature. Pb nanoparticles with average diameter of 23±4nm were prepared by 300 keV Pb ion implantation into thermally grown silica to a fluence of $1x10^{16}$ Pb/cm^2, followed by a two step thermal annealing [1]. Irradiations were performed in-situ at the CSNSM, Orsay, using the ARAMIS accelerator, coupled to the TEM of the JANNuS platform, which enabled us to follow the evolution of the irradiated NP in real time.

The advantage of the in-situ observation is that a single NP can be followed over a large range of irradiated fluences. After an irradiated fluence of $2x10^{15}$ ions/cm^2, 3 nm diameter sattelite NPs are observed. As the fluence is increased up to 5x1015, the satellite diameter increases to 4 nm. At this stage, the original NP has shrunk from 23 down to 16 nm diameter. For higher fluences, the satellites themselves act as secondary sources of Pb, and start to reduce in size. The formation and dissolution of satellites is discussed and interpreted on the basis of Monte-Carlo simulations of the interaction of the NPs with the ion beam performed the SRIM code and the theoretical models [2]. In situ observations of a high temperature annealing of the irradiated samples reveals that the satellites remain stable up to 1100 ºC, contrary to what would be expected from classical OR behavior. Our results suggests that the satellite's composition is different from the original NP, possibly consisting of by some Pb oxide, with lower surface energy than the original metallic NP [3].

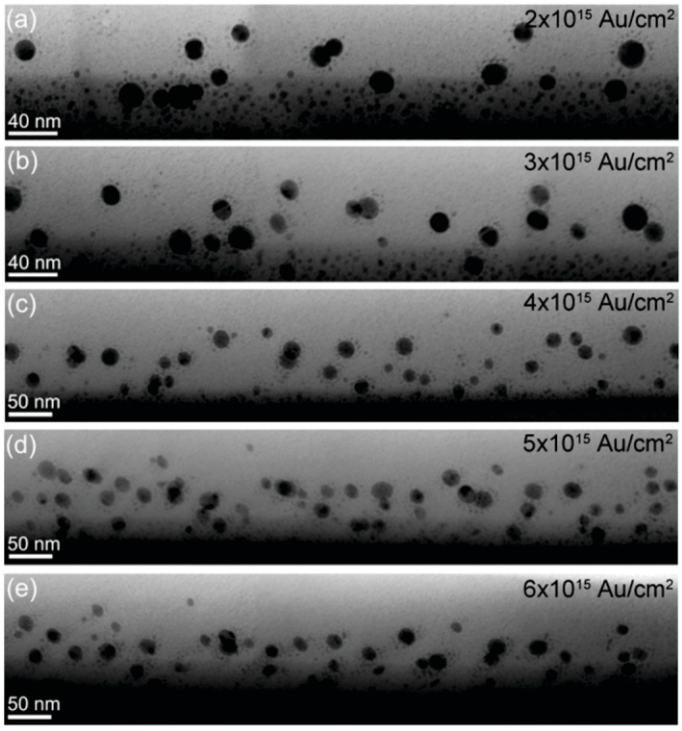

Figure 1 - *Overview of a wide field of irradiated nanoparticles, followed in situ, and shown for selected fluences.*

Publications

[1] F. P. Luce, et al,.J. Appl. Phys. **109**, 014320 (2011)
[2] K. H. Heining et al., Appl. Phys. **A 77**, 17 (2003)
[3] F. P. Luce, PhD Thesis, *Estabilidade de nanopartículas em sílica: efeitos térmicos e de irradiação com elétrons e íons energéticos.* IF-UFRGS 2012

Thermal stability of the Al_2O_3/Ge interface

C. Krug

Introduction

Germanium is being considered a potential candidate to replace silicon (Si) as the channel material for sub-22-nm metal-oxide-semiconductor field-effect transistors (MOSFETs). While higher intrinsic carrier mobilities are attractive, an efficient surface passivation strategy for Ge is still a challenge. Aluminum oxide is a promising candidate for Ge passivation as, among other properties, it presents high thermal stability, large band gap, and adequate conduction band offset to Ge. We investigated the interaction of reactively sputter-deposited Al_2O_3 layers with Ge and the effects of post-deposition thermal annealing in Ar or forming gas at 350°C for 30 min.

Results

The deposition process produces GeO_2 that is readily removed after annealing of the final structure in different atmospheres. The remaining transition layer consists essentially of aluminum germanates, which are present in lower concentration compared to silicates formed in Al_2O_3/Si samples. In Si samples, thermal annealing promoted intermixing of the semiconductor substrate and the dielectric film, which was not the case with Ge. Except for Ge incorporation to the dielectric layer in samples submitted to annealing in Ar, there was no difference between thermal treatment in Ar and forming gas atmospheres.

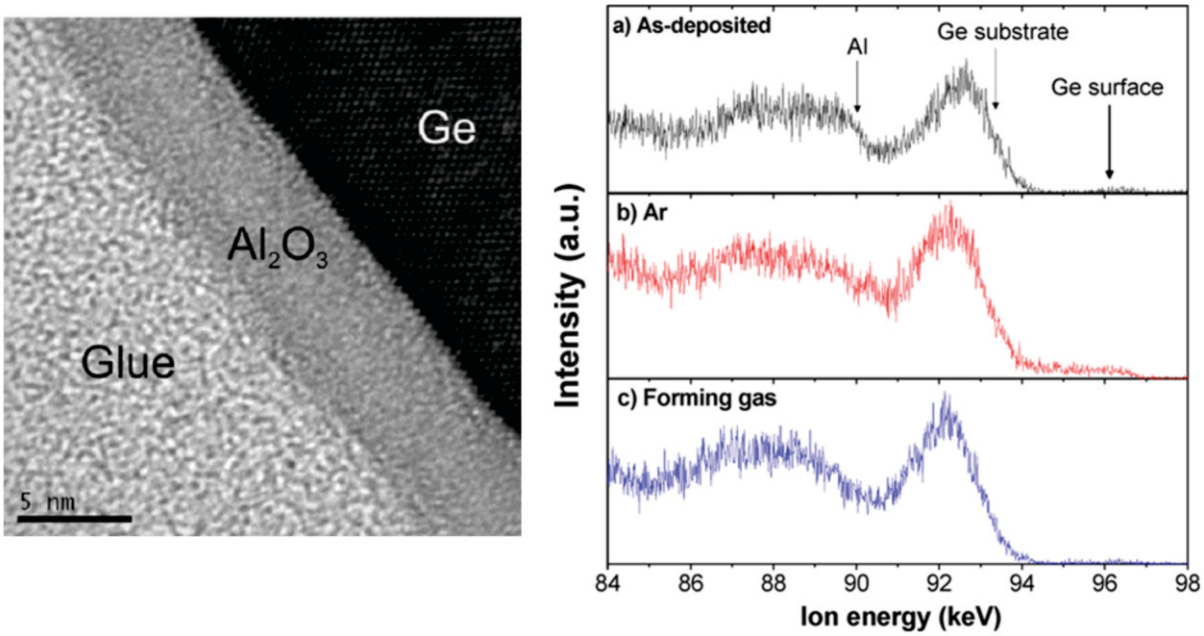

Figure 1 - *(Left) Cross-sectional TEM image of the as-deposited Al_2O_3 layer on Ge. (Right) MEIS spectra from the as-deposited sample (a) and from the same sample after annealing in argon (b) and forming gas (c) at 350 °C for 30 min.*

Research Outlook

Our results evidence that Al_2O_3 in contact with Ge is more stable than in contact with Si, at least in the absence of oxidizing agents, which are known to promote Ge diffusion into the dielectric layer. Thus, Al_2O_3 holds as a promising passivation material for Ge-based devices. Further investigation will focus on the possible role of hydrogen concerning thermal stability of the Al_2O_3/Ge interface.

Publications

[1] N. M. Bom et al., *Evolution of the Al_2O_3/Ge(100) interface for reactively sputter-deposited films submitted to postdeposition anneals*, Appl. Surf. Sci. **258**, 5707 (2012).

Hydrogen interaction with HfO_2 films deposited on Ge(100) and Si(100)

G.V. Soares

Introduction

Germanium is one of the most promissing canditades to replace silicon in high performance metal-oxide–semiconductors field effect transistors. However, the formation of a stable, chemical and electrical passivating dielectric layer on Ge surfaces is still a challenge. HfO_2 is one of the most promising dielectrics for applications in Ge technology, however it has been reported that HfO_2 films on Ge present a high interface state density. Previous theoretical and experimental works have shown that Ge dangling bonds that may exist at the GeO_2/Ge interface cannot be effectively passivated by forming gas annealing (FGA). On the other hand, a significant reduction in Dit figures is observed for gate stacks following FGA. This apparent controversy indicates the need for further understanding of the role played by hydrogen in the electrical and physico-chemical properties of dielectric films on Ge.

Results

Figure 1 shows the D areal density as a function of D_2 annealing temperature for (a) 5 nm and (b) 100 nm thick HfO_2 films deposited on Ge (green squares) and Si (black circles). We observed that D incorporation is higher for films deposited on Si for all investigated temperatures. At 300ºC, a similar difference in D incorporation is observed between films deposited on Si and Ge for both thicknesses. One can say that the main difference between samples is the HfO_2/semiconductor interface region, where D may be incorporated. It can be expected that most of this D is incorporated near the HfO_2/Si interface, where Pb-type defects (silicon dangling bonds) are present. When Ge is used as substrate, the lower D incorporation may be related to theoretically predicated resistance of Ge dangling bonds to hydrogen passivation and/or the theoretically predicated instability of Ge-H bonds.

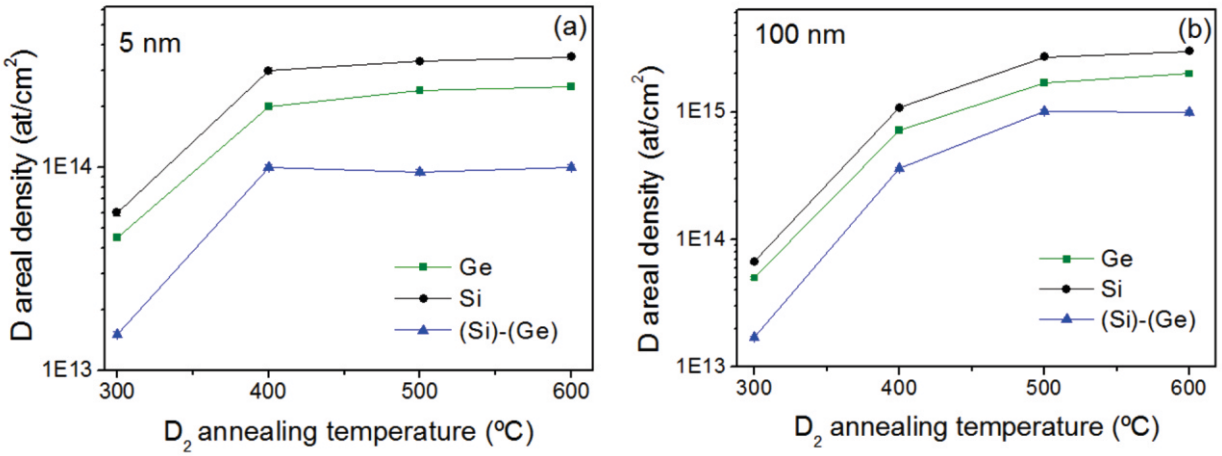

Figure 1 - *D areal density as a function of D_2 annealing temperature for (a)5 nm and (b) 100 nm thick HfO_2 films deposited on Ge (green squares) and Si (black circles). The difference between D areal density in films on Si and Ge is represented by the blue triangles. Lines are only to guide the eyes.*

Research Outlook

Previous reports showed that the use of FGA in the 300-400ºC temperature range presented a reduction in the Dit figures, in such systems as GeO_2/Ge, Al_2O_3/Ge and HfO_2/GeO_xN_y/Ge, corroborating our assumption that most of D is incorporated near the HfO_2/Ge interface region at 300ºC. However, the lower D incorporation when Ge is used as substrate can explain why the passivation is not as effective as in the Si case. One should not disregard that part of this D can be incorporated in the bulk of the HfO_2 film. Future works will focus in the electrical characteristics of theses samples, aiming to understated the role of hydrogen in the electrical properties of the HfO_2/Ge interface.

Publications

[1] G.V. Soares, T.O. Feijó, I. J. R. Baumvol, C.Aguzzoli, C. Krug, and C. Radtke, *Hydrogen interaction with HfO_2 films deposited on Ge(100) and Si(100)*. ECS Transactions, in press (2012).

Sputtered Si_3N_4 films for non volatile memory applications

M. C. Adam, A. V. P. Coelho and H. Boudinov

Introduction

The present work reports the preparation and the electrical and compositional characterization of silicon nitride reactive RF-sputtered thin films. Argon and nitrogen mixtures have been used in different concentrations to optimize the film electrical proprieties. Current-voltage and capacitance-voltage measurements were performed. Furthermore, the films thicknesses and compositions was obtained by Medium Energy Ion Scattering (MEIS). Complete memory structures were fabricated and a program/erase voltage shift window of 10V was measured.

Results

Two different gas mixtures are used for the depositions of the samples A and B. Compositional properties were measured by MEIS. Figure 1 shows MEIS experimental and simulated data for both samples. In Table I are summarized the extracted results for two layer structures (top layer shows oxygen incorporation). Figure 2 shows the memory effect in a capacitance-voltage graph for sample A and sample B fabricated memories. The chosen parameters to program and erase the device are, respectively, 25V and -18V. The pulse width was 10s for both processes. The Memory B has a 10V program/erase window, while the Memory A has approximately 4V. This big difference is attributed to a higher excess silicon concentration in the nitride of memory B, providing better charge trapping behavior.

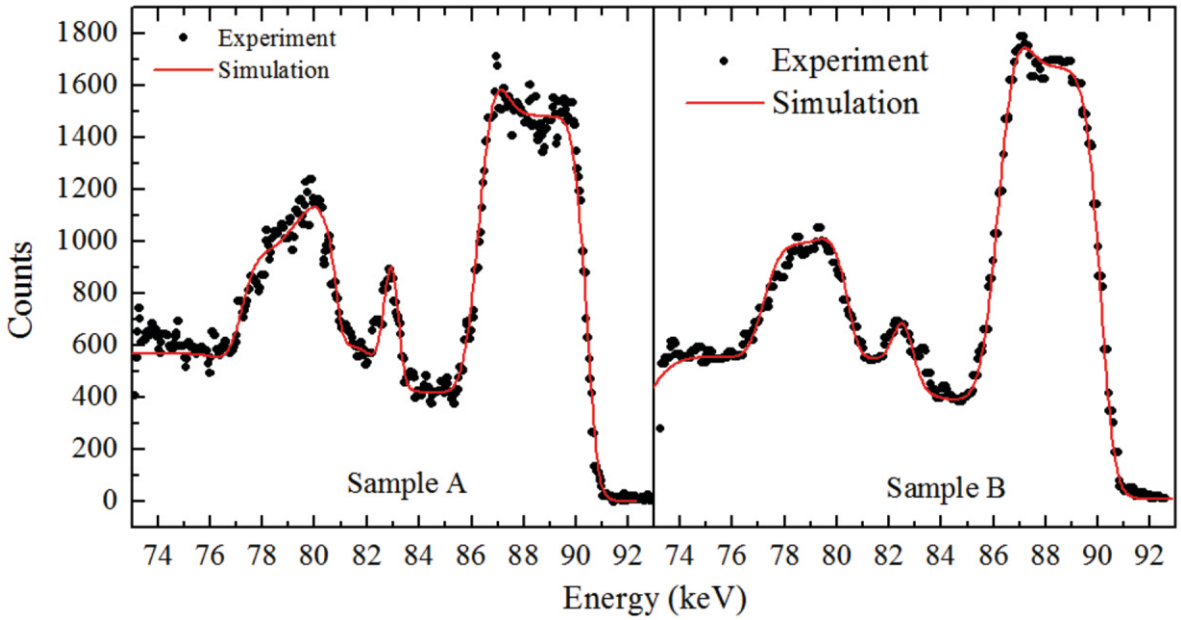

Figure 1 *MEIS experimental and simulated data for samples A and B.*

Table I *Results from simulated MEIS data of samples A and B .*

Sample	Layer	Atomic Composition			Thickness (A)
A	Surface	Si 1	N 2.0	O 2.5	12
	Nitride	Si 3	N 4.6		65
B	Surface	Si 1	N 1.2	O 1.0	12
	Nitride	Si 3	N 3.6		58

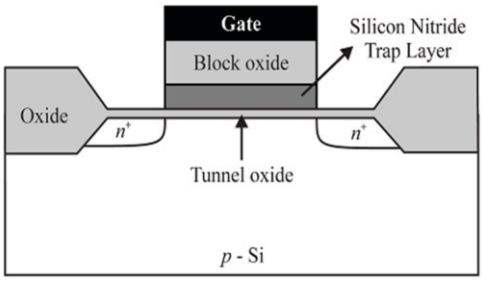

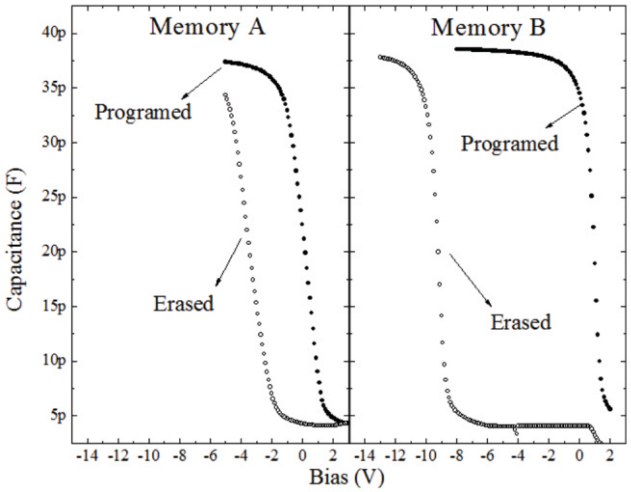

Figure 2 Memory structure (left). Capacitance-voltage characterization of the fabricated memories (right).

Publications

[1] M.C. Adam, A.V.P. Coelho, M.B. Pereira, H. Boudinov. *Sputtered Silicon Nitride Thin Films for Non Volatile Memory Applications*, ECS Transactions, **39**, 371 (2011)

Minimizing the electrical degradation from thermal oxidation of the SiO_2/SiC interface

F. C. Stedile

Introduction

The advances in reducing the interface state density (Dit) between the silicon carbide (SiC) substrate and a SiO_2 film allowed metal-oxide-semiconductor (MOS) devices based on SiC to be commercially available recently. Nevertheless, channel mobility of SiC devices is still very low when compared to the SiC bulk value. Thus, further improvements must be reached such that SiC based devices can achieve larger channel mobility. Minimizing the electrical degradation due to the SiC thermal oxidation seems to be an important step to achieve this goal. It is known that longer oxidation times lead to larger electrical degradation. To minimize the electrical degradation caused by thermal oxidation, a very thin and stoichiometric SiO_2 film was thermally grown. In order to obtain a thicker oxide film, SiO_2 was then deposited by sputtering.

Results

X-ray photoelectron spectroscopy (XPS) analyzes of samples oxidized for short oxidation times are presented and compared to a sample without any thermal treatment in Figure 1. The clean and the first stage of oxidation samples present silicon bonded to oxygen and/or carbon in different stoichiometries, named silicon oxycarbides (SiC_xO_y). As oxidation progresses in time, stoichiometric SiO_2 is the main compound observed. For being the shortest oxidation time investigated to grow a stoichiometric SiO_2 film, 5 min was the oxidation time condition chosen to thermally grow the SiO_2 film before the deposition.

Figure 2 presents the electrical measurements of MOS structures formed by different routes. It is possible to observe that the sample with 5 minutes oxidation prior the deposition presented the best electrical dielectric properties and lowest effective negative charge.

Results indicate that the short oxidation time reduced the electrical degradation in the SiO_2/SiC interface and the oxide deposition decreased the

the amount of effective negative charge as compared to the sample only thermally oxidized.

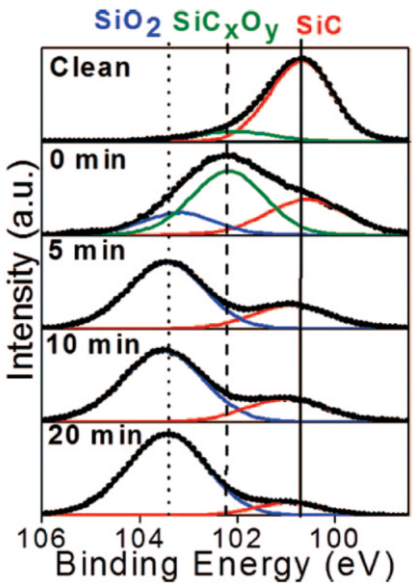

Figure 1 - *Si 2p photoelectron spectra (a.u. stands for arbitrary units) at a take-off angle sensitive to the surface of Si-faced 4H-SiC samples thermally oxidized at 1100°C in 100 mbar of $^{18}O_2$ for different oxidation times, as indicated. Vertical lines indicate the presence of the compound appearing in the top of the figure: SiC (solid), SiC_xO_y (dashed), and SiO_2 (dotted).*

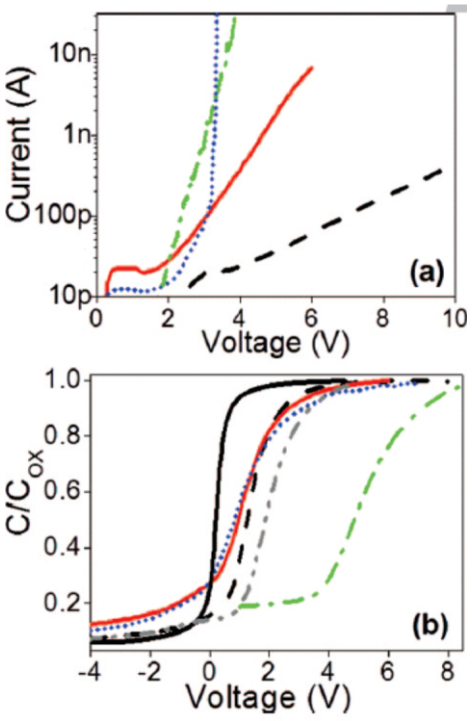

Figure 2 - *(a) I-V curves and (b) C-V curves of Al/SiO_2/4H-SiC (Si face) structures. 20 nm SiO_2 films deposited by sputtering on SiC not submitted (dotted-dashed green lines) and submitted (dotted blue lines) to annealing in Ar (400 mbar for 1h at 1100°C). SiC samples with SiO_2 films thermally grown under 100 mbar of $^{18}O_2$ at 1100°C for 5 min followed by the same SiO_2 deposition not submitted, leading to a film 23 nm thick (dashed black lines), and submitted (solid red lines) to the same Ar annealing. Ideal C-V curve (solid black line) and the curve of a SiC wafer oxidized under 100 mbar of $^{18}O_2$ at 1100°C for 4 h (dot-dot-dashed gray line), leading to a film 14 nm thick, are also presented for comparison.*

Research Outlook

The presented results indicate that the route to obtain the SiO_2 film on SiC has a major impact in the electrical properties of MOS structures and that short thermal oxidation followed by SiO_2 film deposition is a good choice, leading to better electrical properties of the structures.

Publications

[1] Eduardo Pitthan, Rodrigo Palmieri, Silma A. Corrêa, Gabriel V. Soares, Henri I. Boudinov, Fernanda C. Stedile, *The Role Played in the Improvement of the SiO_2/SiC Interface by a Thin SiO_2 Film Thermally Grown Prior to Oxide Film Deposition*, ECS Solid State Letters, vol. **2**, page P8 (2012).

Raman and TEM Characterization of Ion Beam Synthesized SiC on Insulator

R.L. Maltez

Introduction

Silicon Carbide (SiC) is a promissing semiconductor for high-power and high frequency electronic devices. It is also appropriate to work in reactive environments due to the strong bonding between Si and C. Ion Beam Synthesis (IBS) is an attractive method to obtain 3C-SiC layers on Si. In addition, SiC has been used as buffer layer for further growth of other well-matched materials like GaN and ZnO. Therefore, conversion of a thin surface layer of low cost Si wafers into SiC would be an alternative integration route between such materials and Si technology. In this work, Raman spectroscopy was applied as a tool to observe the formation of C-C bonds in a nanometrict SiC (40 nm) synthesized on the SiO_2/Si structure. Samples were investigated as a function of the implanted C fluence adopted for the synthesis. Raman technique is capable of differentiate signals of crystalline carbon regions from highly disordered ones and it is also sensitive to the C hybridization. Transmission electron microscopy (TEM) analysis was employed to characterize the synthesized structures, presenting a direct observation of the SiC crystalline quality differences.

Results

Raman spectra of carbonaceous materials show two quite strong vibration modes, the G peak around 1580cm^{-1} and the D peak around 1350 cm^{-1}, both features of the C-C sp^2 bonds. In addition to the R parameter ($R=I_D/I_G$) usually defined in the literature, a new parameter (named RC) was defined as the ratio of the spectrum area in the wavenumber range from 1100 up to 1700 cm^{-1} (where the peaks D, D2 and G can be found, all related to C bonds contributions to the Raman spectra) by the area under the peak corresponding to the bulk crystalline Si substrate structure (520 cm^{-1}).

R and RC parameters for analyzed samples are summarized in Table 1 where we also present the Lorentzian fittings for all samples, showing the wavenumber value and the FWHM of both D and G peaks.

RC parameter appears to be more sensitive to changes in the crystal quality: it shows 315% and 870% increases for the annealed samples high fluence SIMOX65 and high fluence SIMOX35, respectively, in relation to the value of the annealed low fluence SIMOX65. The high sensitivity of the RC parameter, in addition to its simple interpretation as being proportional to the amount of C-C bonds formed in the SiC layer, where we should have just Si-C bonds in a perfect crystal, makes the RC a good additional parameter to relatively probe the crystalline quality among nanometric SiC layers formed on Si substrates, when the Si-C direct signal is very weak or null in the spectra.

Sample	Peak	Wavenumber (cm^{-1})	FWHM (cm^{-1})	R (I_D/I_G)	R_C ($I_{Carbon}/I_{Silicon}$)
Low fluence SIMOX65 annealed	D G	1365 1579	211 193	1.1	0.14
High fluence SIMOX65 As-implanted	D G	1411 1558	232 178	-	0.19
High fluence SIMOX65 annealed	D G	1348 1565	160 240	1.3	0.58
High fluence SIMOX35 As-implanted	D G	1450 (single peak)	- -	-	0.44
High fluence SIMOX35 annealed	D G	1341 1558	185 160	2.3	1.35

Table 1: *RAMAN analysis summary. Wavenumber values and FWHM for D and G peaks and R and RC ratios for each spectrum.*

The conclusion drawn through RC parameter was the same that obtained through R parameter: low fluence SIMOX65, high fluence SIMOX65 and high fluence SIMOX35 are, in this order, the increased damage sequence. Structural quality was independently verified by TEM analysis, and it is in total agreement with the results obtained from Raman spectroscopy represented by R and RC parameters.

Research Outlook

Studies on Ion Beam Synthesis of SiC by C implantation in Si(111) substrates are in progress in order to improve the structural quality of synthesized layers. SiC synthesis on pre-implanted Si with He ions were performed. Interaction between the He pressurized buried layer and the SiC layer under formation are being investigated.

Publications

[1] R.M.S. dos Reis, R.L. Maltez, E.C. Moreira, Y.P. Dias, H. Boudinov, *Raman and TEM characterization of high fluence C implanted nanometric Si on insulator*, Applied Surface Sience, **258**/19, 7395–7400 (2012)

Ne-He bubble formation in co-implanted Si(111) substrates

R.L. Maltez

Introduction

It was reported in a previous work [1,2] that formation of over-pressurized bubbles in a Si(111) substrate is able to improve the crystalline quality of GaN/AlN (AlN is a buffer layer) structures heteroepitaxialy grown on it. The bubbles band in the substrate attracts the misfit dislocations generated at AlN/Si and GaN/Si interfaces and redirects them toward the substrate, thus reducing the dislocation density in the overgrown GaN layer. We are now investigating Si(111) samples containing Ne and Ne-He bubbles obtained from different implantation parameters and annealing temperatures (Ne bubbles are stable at high temperatures). Our final purpose is to find bubble systems able to keep comparable pressure to the He case even at higher temperature than the 650°C threshold of He. This requires understanding of which parameters play fundamental role on defining the morphology and pressure in such co-implanted system. Ne implantation was performed with the sample kept at 350°C to reduce implantation damage. These samples were submitted to RTA annealing for 2 minutes in the 400 to 1000°C temperature range. Characterization by Rutherford Backscattering Spectrometry/Channeling (RBS/C), Elastic Recoil Detection (ERD) and Transmission Electron Microscopy (TEM) are employed.

Results

We have found that bubbles are always present in Ne-He hybrid system, even after annealing at 1000°C. However, while bubbles have increased in size as increasing the annealing temperature, the channeling in the samples has rather improved. It is an opposite behavior to the one expected if the dechanneling was a consequence of over-pressurized bubbles: the channeling degree in the samples should be worst during bubbles coarsening. In this sense, by RBS/C we do not observe clear correlation of dechanneling as a result of bubble formation for all investigated temperature range.

An special set ($1x10^{15}$ cm^{-2} Ne and $1x10^{16}$ cm^{-2} He), however, has showed slightly different thermal behavior, mainly for the annealing temperatures of 400 and 600°C: they show channeling spectra whose dechanneling in the implantation depth overcomes the as-implanted one. In addition, this specific co-implantation set and temperatures also demonstrated a peak shape for the dechanneling which resembles the one observed for the He pure case.

However, we have observed a consistent correlation between channeling improvement and implantation damage reduction, suggesting that defects are the main cause of the observed dechanneling for the systems containing Ne. From TEM analysis it was also clear that bubbles in the hybrid system are all spherical ones and does not recall any similarity to the He system, even with Ne:He ratio of 1:10. Thus, from a morphologic point of view, the He and Ne hybrid system is very alike to Ne pure bubbles for the chosen implantation paramaters.

Research Outlook

Since residual implantation damage plays an important role on defining the pressure and morphology of such co-implanted system, the next step is aiming to an almost total damage annihilation during the implantation. Increasing of the sample implantation temperature and also interchange the implantation order of the Ne and He ions are the present status of the investigation.

Publications

[1] Z. Liliental-Weber, R. L. Maltez, J. Xie, e H. Morkoc, *Propagation of misfit dislocations from AlN/Si interface into Si*, Journal of Crystal Growth, **310**, 3917 (2008)
[2] Z. Liliental-Weber, R. L. Maltez, J. Xie, e H. Morkoc, US patent # 8,008, 181
[3] L.G. Matos, R.M.S. dos Reis and R.L. Maltez, *Ne-He bubble formation in co-implanted Si(111) substrates*, Submitted to Thin Solid Films.

Two band photoluminescence emission from Si nanocrystals in SiO_2 matrix

A.E.P. Mattos, P.L. Franzen, M. Girotto and H. Boudinov

Introduction

Silicon rich SiO_2 samples were prepared using reactive RF sputtering from Si target. By controlling the oxygen concentration of the $Ar + O_2$ mixture in the deposition chamber, an excess of silicon was created in the formed silicon oxide films. After performing a thermal annealing at temperatures of 1050ºC and 1100ºC, these samples showed a photoluminescence (PL) effect, which was caused by the formation of silicon nanocrystals. The PL signal was observed when the samples were excited with the 488 nm line of an argon laser. Significant improvement of the PL signal was achieved by subsequent thermal annealing at 450ºC in forming gas (FG), which passivates the silicon nanocrystals interfaces. PL measurements as a function of the laser power permitted to distinguish between two different mechanisms of light emission.

Results

It is known that several parameters can contribute to light emission from silicon nanocrystals (Si-nc). Two important characteristics of the PL signal are the number and the size of Si-nc. Additionally, in the interface between silicon and the isolator, defects and impurities contribute to nonradiative transitions. The shape of PL signal spectra is correlated with the nanocrystals size distribution. Large grains will contribute for longer wavelengths and the small ones will contribute to shorter wavelengths. The PL spectra after second annealing in FG for different laser powers are shown in Figure 1. Two mode PL emission is observed for all curves.

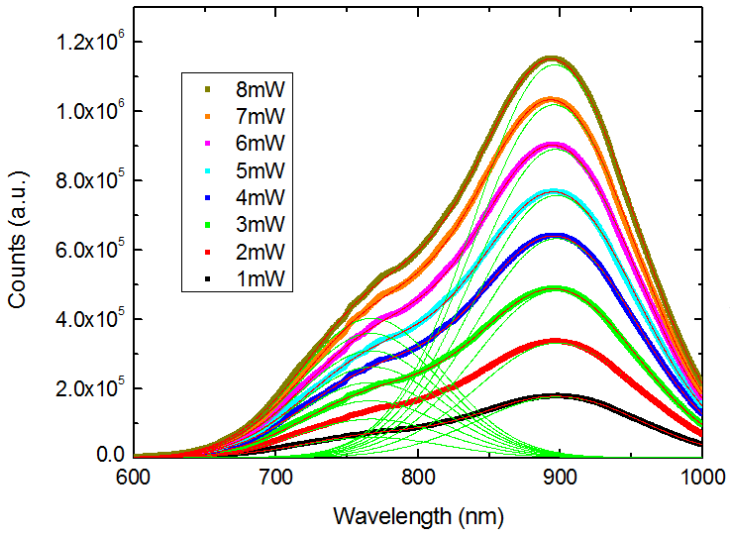

Figure 1 - *Photoluminescence spectra with different power excitation, varying from 1mW up to 8mW. Fitted curves (red) are shown as a sum of two Gaussian curves (green) centered at 760 nm and 900 nm for all spectra.*

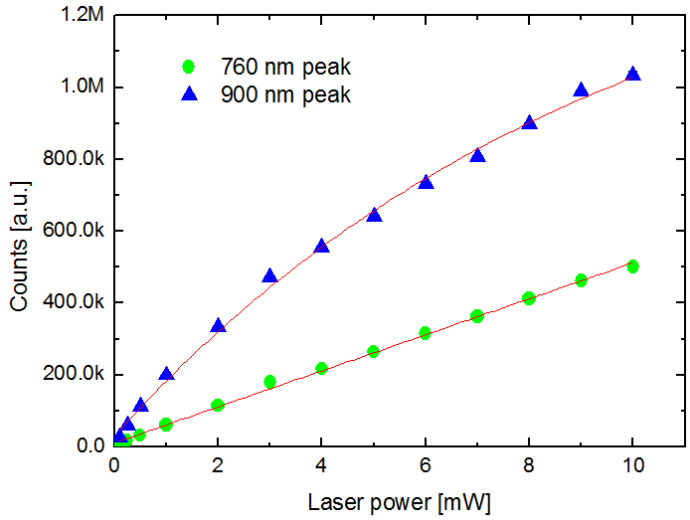

Figure 2 - *Photoluminescence peaks intensities as functions of the laser power. The higher energy peak (760 nm) is linearly dependent, but a nonlinearity is observed for the second one (900 nm).*

Research Outlook

It is assumed that the left peak is related to the quantum confinement of Si-nc, while the right one is related to the radiative recombination of localized levels formed by interface states on the Si-nc/SiO_2 interface. The PL peak intensities dependences in Fig. 2 confirm that two different mechanisms are responsible for both peaks PL emissions, due to the fact that one of them is linear with the laser power and the second one shows a saturation tendency for this power regime.

Publications

[1] A.E.P. Mattos, G. Sombrio, P.L. Franzen, M.B. Pereira, H. Boudinov. *Si Nanocrystals Embedded in SiO_2 Produced by Reactive Sputtering for Light Emission*, ECS Transactions, 39, **103** (2011)

UV photoluminescence emission from Si rich Si_3N_4

G. Sombrio, P.L. Franzen and H. Boudinov

Introduction

Silicon is by far the most used material in the microelectronics industry, the reason for this preference being its excellent electrical and mechanical properties. However, for being an indirect band gap semiconductor it is a poor light emitter. Many attempts were made to eliminate this obstacle and the problem is a subject of continuing research. Some of the most promising results were obtained by creating silicon nanostructures embedded in dielectric materials, such as silicon quantum dots, erbium doped silicon and porous silicon. Those low dimensional structures disturb the band gap configuration, increasing the radiative recombination rate of the excitons, resulting in improved light emission.

In this work, we used samples prepared by reactive sputtering to create layers of non-stoichiometric silicon nitride. By carefully controlling the amount of nitrogen, argon and oxygen mixture in the sputtering chamber, the temperature and time of annealing, we have controlled the composition and the subsequent photoluminescence spectra. For the first time a strong UV (324 nm) emission was observed in a $Si_3N_xO_y$ sample with a relatively high oxygen concentration.

Results

Three samples with different compositions (see Table I) are prepared by RF sputtering. The PL measurements were realized at room temperature using a 266 nm CW Solid State Laser as an excitation source. The laser power was kept at 1 mW. The photoluminescence spectra of these samples are shown in Fig.1.

Table I *Compositions of the sputtered samples (RBS measurements)*

Sample	Si(%)	N(%)	O(%)
A	43	57	-
B	31	56	13
C	32	22	46

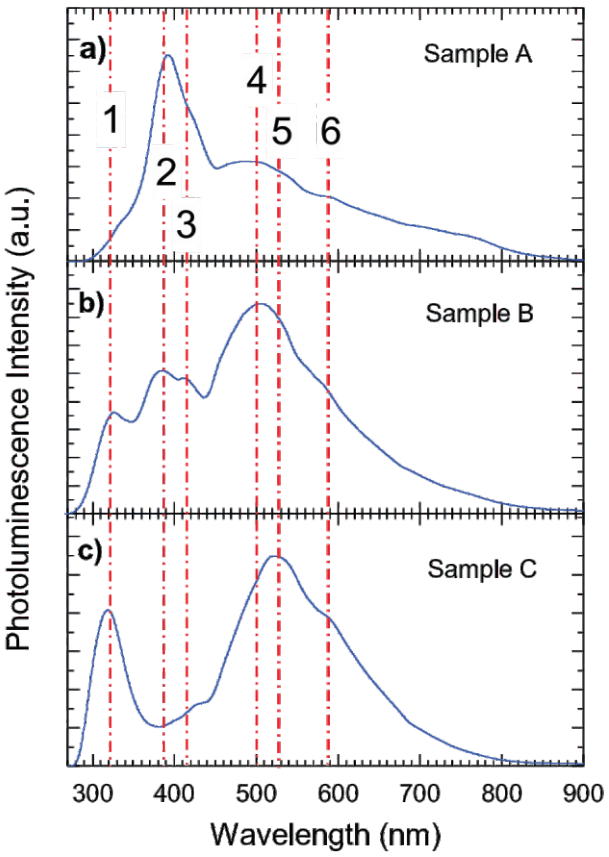

Figure 1 - *Photoluminescence spectra of $Si_3N_xO_y$ from the samples with compositions shown in Table I. The peak 2 (3.2 eV) and peak 3 (3.0 eV) are more pronounced in the samples with less oxygen concentration and are related to silicon and nitrogen dangling bonds defects, respectively. The UV peak 1 (3.8 eV) is increasing with the oxygen incorporation and was not observed till now in similar structures. The peaks 4,5 and 6 have a similar behavior like peak 1 in relation to the oxygen concentration, but these are very well known emissions from Si-nc/Si_3O_x system.*

Research Outlook

The reactive sputtering technique from Si target was employed for the fabrication of $Si_3N_xO_y$ samples and an UV PL emission was observed for the first time from similar structure. Electroluminescence measurements could provide valuable additional information for the complex band configuration in this material and the possibility to design a new kind of UV LED is rising.

Publications

[1] G. Sombrio, A.E.P. Mattos, P.L. Franzen, M.B. Pereira, H. Boudinov. *Photoluminescence in Non-Stoichiometric Silicon Nitride Films Obtained by Reactive Sputtering*, ECS Transactions, **39**, 315 (2011)

Photoluminescence from Tb and Eu implanted at high temperature

F. L. Bregolin, U. S. Sias and M. Behar

Introduction

Recently in our group, it was demonstrated that Si and Ge nanoparticles, obtained by using the ion implantation technique performed at high temperature (hot implants), present higher photoluminescence (PL) yields than those implanted at room temperature (RT). The present work deals with the PL emitted from Eu and Tb ions implanted from (RT) up to 350°C in a SiO_2 matrix, followed by a further anneal process. The ions were implanted with energy of 100 keV and a fluence of $3x10^{15}$ ions/cm². Further anneals were performed in atmospheres of N_2 or O_2 at temperatures ranging from 500 up to 800 °C. PL measurements were performed at RT and structural measurements were done via transmission electron microscopy (TEM). In addition, the Rutherford backscattering technique (RBS) was used to investigate the corresponding ion depth profiles.

Results

- Tb results. As shwon in Fig. 1 with increasing implantation temperatures, there is an increase of the PL emission, being the minimum for the RT and maximum for 350 °C. Concerning the annealing temperature, the maximum is observed at 500 °C regardless of the implantation temperature. However, the maximum PL yield is observed at a combination of a hot implant at 200 °C and anneal at 500 °C. The TEM images (not shown) has revealed that the 350°C implantation provides sufficient thermal energy for the precipitation of nanoparticles during the implantation process.
- Eu results. For samples implanted at RT and 200 °C, the PL intensities are practically the same. On the other hand, the samples implanted at 350 °C present a 20 % increase in the PL intensity of the lines that are in the red region of the spectrum, and 45 % for the blue-green PL band, as compared with the ones implanted at RT. After the thermal treatments, all the spectra present a broad emission band from 370 up to 850 nm, differing significantly from the PL emission characteristics of the as-implanted sample –see Fig. 2 (on the left).

The TEM images – Fig. 2 (on the right) - reveal that the 350 °C

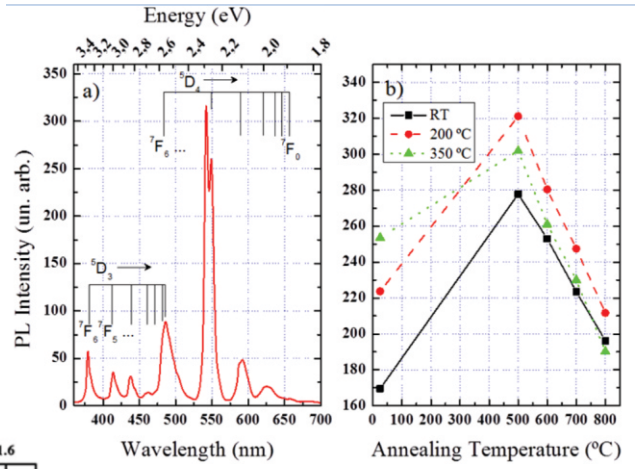

Figure 1 - *a) Typical spectrum of a Tb implanted sample, showing the radiative electronic transitions of the Tb ions. b) PL intensity of the 542 nm line as function of the annealing temperature for samples implanted at RT, 200 and 350 °C.*

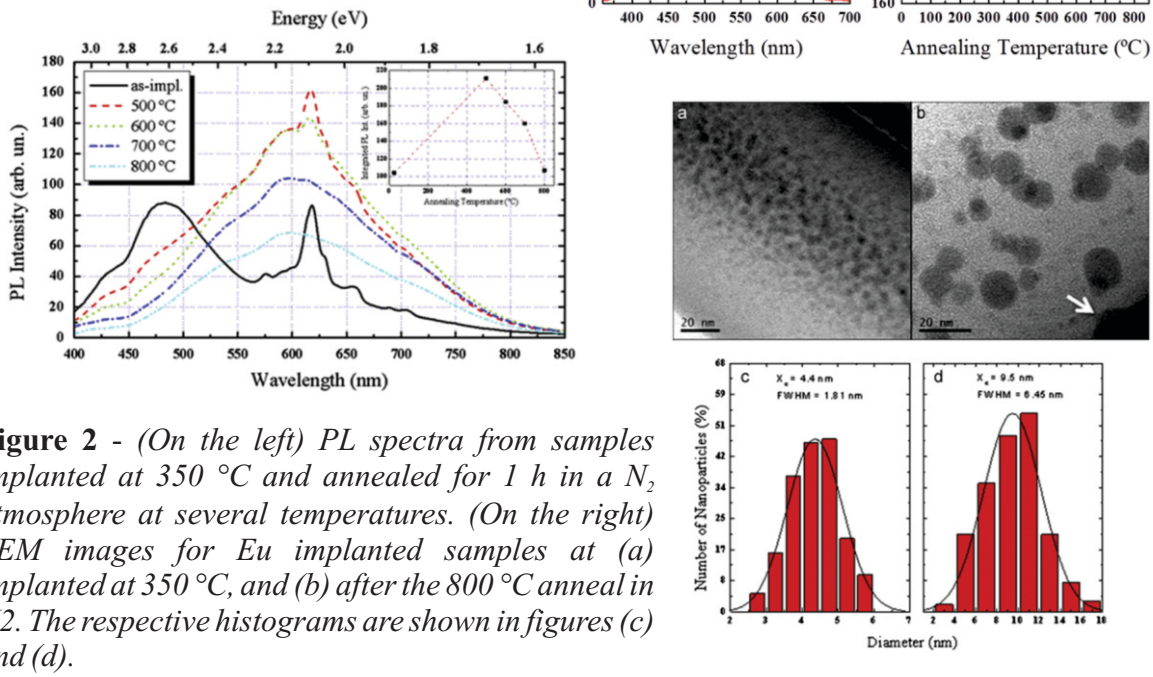

Figure 2 - *(On the left) PL spectra from samples implanted at 350 °C and annealed for 1 h in a N_2 atmosphere at several temperatures. (On the right) TEM images for Eu implanted samples at (a) implanted at 350 °C, and (b) after the 800 °C anneal in N2. The respective histograms are shown in figures (c) and (d).*

implantation provides sufficient thermal energy for the precipitation of Eu nanoparticles during the implantation process. Before the anneals, no nanoparticle was observed for the samples implanted at RT. At variance with what was observed for Tb, the annealing atmosphere plays a major role in the Eu PL results. In fact samples annealed in N_2 presented a broad PL band, ranging from 370 up to 840 nm. On the other hand, the O_2 anneal conserves the original shape of the as-implanted spectra, that is: a broad PL band in the blue-green region together with sharp PL band in the red region. This feature is due to the strong passivation effect of the oxygen atmosphere together with its influence in favoring the Eu^{3+} state.

Publications

[1] F. L. Bregolin, U. S. Sias and M. Behar, *Photoluminescence and structural studies of Tb and Eu implanted at high temperatures into SiO_2 films*, J. Lumin. (2012) (In Press) - http://dx.doi.org/10.1016/j.jlumin.2012.10.010

Modulating the ZnO nanowire-based gas sensor sensitivity by ion irradiation

D.L. Baptista

Introduction

Metal-oxide semiconductor nanowires have enormous potential in high sensitive, fast and selective sensing applications. It may be used to selectively detect different gases, chemical and biological substances. Single ZnO nanowire-based devices can be used to stably detect very small quantities (p.p.b.) of a certain substance, such as CO, CO_2, O_2, NH_3, H_2, NO, H_2S even at room temperature. Defects, surface morphology and oxygen-adsorption behavior play a crucial role on the device sensitivity. Such sensitivity may also be modulated and enhanced by ion irradiation/implantation at appropriate doses.

In this work, single and multi-nanowire devices were fabricated by electron beam lithography using the Raith e-line system at CBPF. ZnO nanowires were previously grown on sapphire substrate by catalytic vapor phase method and than dispersed in 2-propanol. The solution was dripped on SiO_2/Si wafers and the wires were then contacted by Ti/Au nanocontacts fabricated by lift-off process. Electrical transport measurements were performed in a gas sealed chamber by using a Keithley 2612A system. The nanowires were irradiated with He ions at 1.2 MeV in several fluencies from 10^{13} to 10^{16} He.cm^{-2}. Native and irradiation-induced point-defects in the ZnO wurtzite structure were monitored through PL measurements carried out at room and low (down to 12 K) temperatures using a 266 nm CW Laser. High-resolution TEM was also performed using a Titan 80-300 microscope aiming to probe crystallographic characteristics.

Results

The results show a relative intensity decrease of whole PL defect-level visible emission band concern the UV near-band-edge for intermediate ion fluences. It indicates an enhanced dynamic annealing effect during irradiation allowing it to heal low migration barrier point-defects such as oxygen interstitials (O_I), zinc interstitials (Zn_I), zinc antisites (ZnO) and

relative increase of the 1.7 eV emission with the ion fluence. This short-infrared emission starts to rise at 100K (enhanced by the freezeout regime) and it is believed to be a deep donor state directly related to oxygen vacancies (V_O), which present higher stability (higher migration barrier energy).

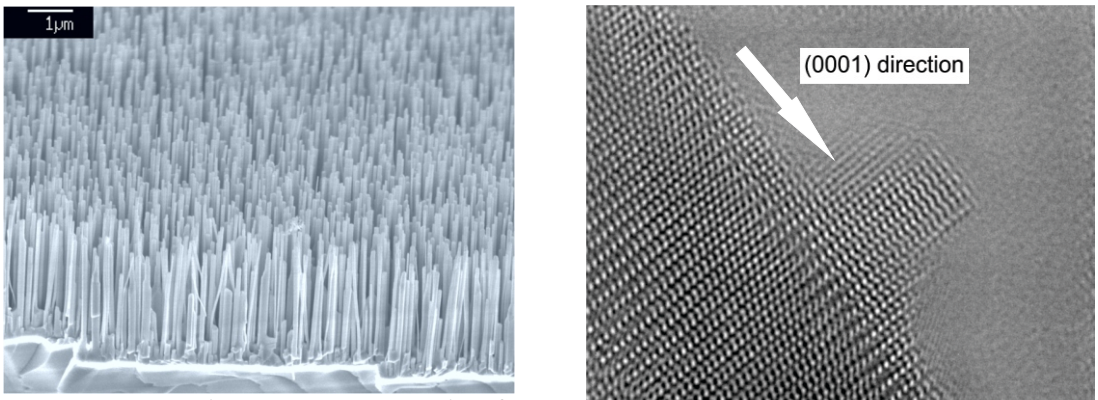

Figure 1 *Scanning electron micrograph of ZnO nanowires forest (on left). HRTEM of an individual ZnO nanowire showing the hexagonal wurtzite atomic structure.*

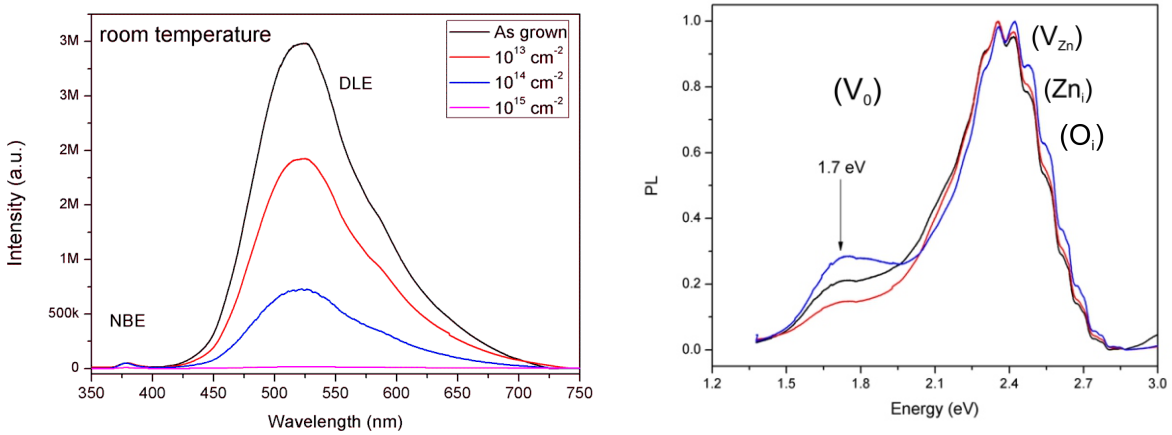

Figure 2 *(left) Photoluminescence of ZnO nanowires subjected to ion irradiation with different fluencies. The spectra show the NBE and DLE peaks. (rigth) Low temperature (12 K) DLE photoluminescence of ZnO nanowires subjected to ion irradiation with different fluencies. The short-infrared emission at 1.7 eV is outstanding.*

Research Outlook

Native and induced point-defects seems to play a major influence on the modulation of the gas detection sensitivity of ZnO nanowire-based devices. Thus, ion irradiation is able to modulate the nanowire electron concentration and therefore exerting influence on the deplection/accumulation regimes, which are responsible for the sensor activity

Publications

C. I. Lisevski, A. L. F. Cauduro, P. L. Franzen, H. I. Boudinov and D. L. Baptista, *Electrical and Optical Behavior of ZnO Nanowires Irradiated by High-energy Ions*, SBMicro 2013.

Nanostructured tungsten oxide thin films obtained through thermal evaporation

I. T. S. Garcia

Introduction

Tungsten oxides (WOx) are unique materials that have been rigorously studied for their chromism, photocatalysis, and sensing capabilities. The obtention of nanostructured oxide is important because the size of particle. WO_3 is a n-type semiconductor, with an electronic band gap, corresponding to the difference between the energy levels of the valence band, formed by filled O 2p orbitals and the conduction band formed by empty W 5d orbitals and, depending on crystalline structure, varies from 3.25 eV to 2.62 eV at room temperatur,e which is useful in photocatalysis. Nanostructured WO_3 films can be obtained through several physical and chemical processes, implying in different structures. We obtained tungsten oxide thin films by thermal evaporation and substrate, temperature and time of deposition. Structure were investigated. Morphology by scanning electron microscopy and chemical composition was evaluated through nuclear reaction analysis $O^{16}(\alpha,\alpha)O^{16}$, also was verified the resistance to lixiviation in aqueous solution (pH = 6).

Results

Nano and microstructured thin WO_3 films were obtained. Films on silicon and Au/Silicon substrates are resistant to lixiviation at pH 6, and are able to support photocatalytical tests in next stage for study. Higher temperatures of substrate are responsible for the nanostructure aggregation which can be seen through SEM micrographs (Fig. 1). Substrate temperature is an important factor, because when we furnish energy to the system, it tends to acquire the morphology with lower surface energy.

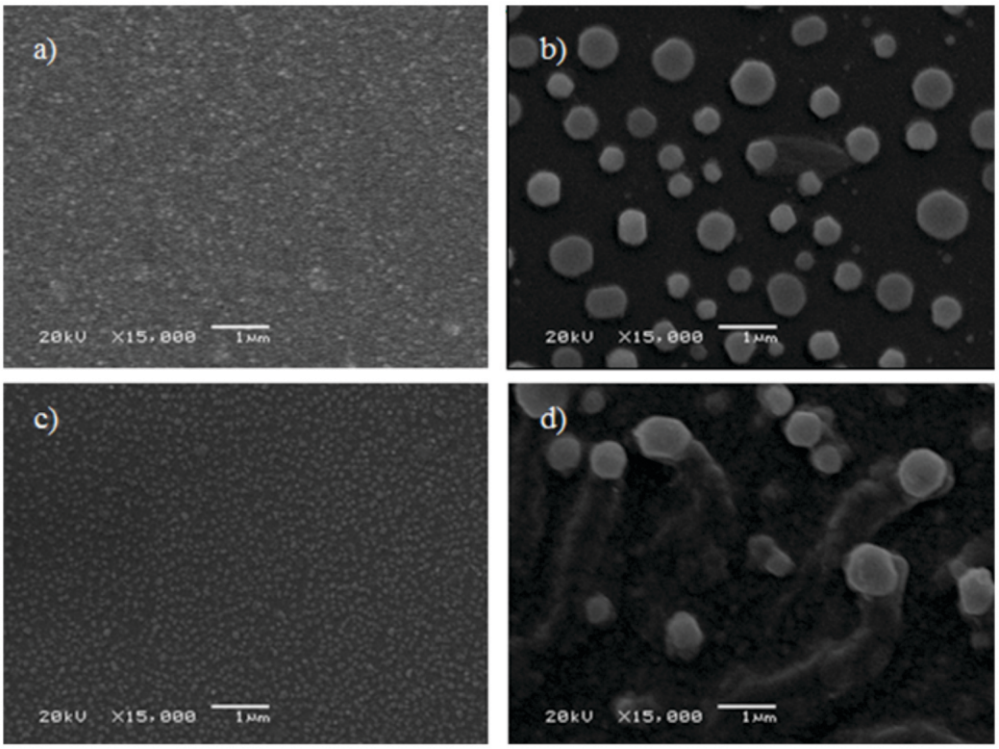

Figure 1 - Micrographs of WO_3 films on silicon substrate covered with gold) 200 ° C, 60 min b) 600 ° C, 60 min, c) 200 ° C, 90 min d) 600 ° C, 90 min.

Research Outlook

The use of ion irradiation as a tool for obtaining well defined optical properties in such systems will be investigated and the band gap of these systems will be modified through chemical doping and ion implantation of transition metals; These modified systems will be characterized with respect to their optical properties: refractive index, absorption coefficient and optical gap. The evaluation of the photocatalytic characteristics will be evaluated in degradation tests of simulated organic effluent.

Publications

[1] D. S. Correa, *Effect of temperature on WOx composition* , to be submitted to Thin Solid Films.

Mechanical properties and physicochemical characteristics of CrN/Si_3N_4 multilayers

C. Aguzzoli, T.P. Soares, G.V. Soares, C.A. Figueroa, I.J.R. Baumvol

Introduction

Protective hard coatings for engineering components and tools based on thin metal nitrides and carbides films are of current use in different applications. Starting from TiN, the materials investigated and used for coated expanded to cover several many others, such as Cr, V, Zr, W, Nb, Al-Ti nitrides and carbides films. According to the material chosen for a specific coating, hardness can be significantly increased, as well as wear, friction and corrosion can be significantly reduced. One must not forget here the applications of coated metals and polymers in applications where biocompatibility is needed.

Multilayered thin film coatings can increase even further the hardness of the coatings, leading in some cases to superhardness (above 40 GPa). Depending on the nature of the components of individual layers, the sub-micron structure, interface width, and the formation mechanisms of the multilayered coating.

Results

The elementary composition of the films was determined by Rutherford backscattering spectrometry (RBS) using He+ ions incident at 2 MeV. The concentration of impurities in the films was determined too, for example O, Fe, Cr, and others are all below the sensitivity limit of RBS. The presence of impurities would affect significantly the hardness and the adhesion of the coatings to the substrate.

The hardness (H) of the multilayers with different bilayer periods (Λ) are shown in Figure 1 for the three different indentation depths. The hardness of the CrN/Si_3N_4 multilayered coatings increased with the increase of Λ from 2 to 4 nm, where the hardness reached its maximum value ($H = 34.6 \pm 1.27$ GPa). For larger Λ, the hardness presented a trend to decrease down to the upper values expected from the rule of mixtures, namely 23 to 26 GPa.

The hardness of the individual CrN (12 GPa) and Si_3N_4 (26 GPa) layers are shown with horizontal lines in Figure 1.

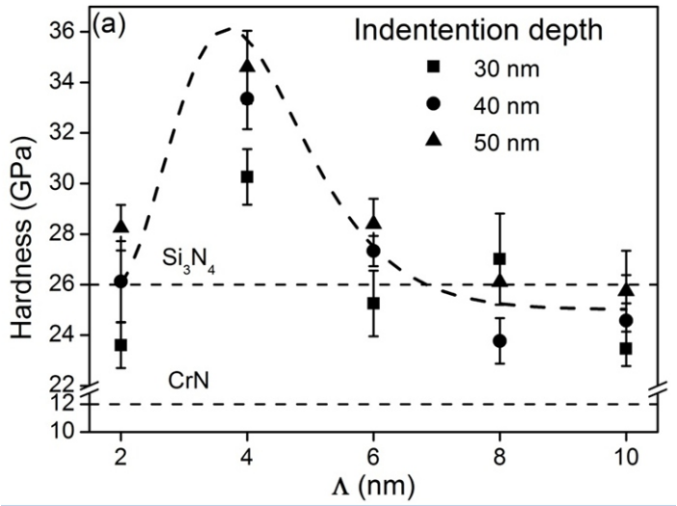

Figure 1 - Hardness (H), for the different CrN/Si_3N_4 multilayer periods (Λ) of the present work. The lines are only to guide the eyes. The hardness of the individual Si_3N_4 and CrN layers are indicated in doted line.

Research Outlook

The hardness increase observed here was not reported in previous works published in the literature. However, these works were performed at deposition temperatures far lower than those corresponding to the maxima hardness of the individual layers, whereas here the deposition were made at a temperature corresponding to the hardnesses maxima, namely 300 °C. It is well known from the literature that superhardness is obtained in multilayered coatings in which at least one of the individual layers is very hard. Therefore, by depositing the present multilayers at temperatures close to the hardness maxima of the individual layers, one could expect to obtain hardness increase.

Publications

[1] C. Aguzzoli, T.P. Soares, G.V. Soares, C.A. Figueroa, ; I.J.R. Baumvol, *Mechanical properties and physicochemical characteristics of CrN/Si_3N_4 multilayers*, Sent to Surface & Coatings Technology, (2012).

[2] C. Aguzzoli, C.A. Figueroa, F.S. de Souza, A. Spinelli, I.J.R. Baumvol, *Corrosion and nanomechanical properties of vanadium carbide thin film coatings of tool steel*, Surface & Coatings Technology, **206**, 2725-2731 (2012).

[3] C. Luvison, V. Sonda, A.C. Rovani, F. Cemin, F.G. Echeverrigaray, C. Aguzzoli, A.E. Crespi, C.L.G. Amorim, M.E.H. Maia da Costa, I.J.R. Baumvol, C.A. Figueroa, *Friction in near surface regions of plain steel plasma-nitrided and post oxidized at various hydrogen contents*, Vacuum (Oxford), **86**, 1268-1272 (2012).

Characterization of thin films of Si_3N_4 containing MoS_2

R. Trentin, A. L. Bandeira, T. P. Soares, C. Aguzzoli, M.C.M. Farias, C. A. Figueroa

Introduction

Currently, thin films are used in a wide range of industrial applications, such as carbides, nitrides and oxides that are applied from the microelectronics industry to the mechanical conformation industry. Silicon nitride (Si_3N_4) is notable for its properties of chemical and thermal stability, exhibiting resistance to temperatures above 1000 °C, hardness of around 22 GPa, and low friction coefficient. For this reason, the thin films of silicon nitride are already applied industrially. In contrast, molybdenum disulfide (MoS_2) acts as a solid lubricant with excellent results in vacuum environments, so it is widely used in the aerospace industry in conjunction with other materials. Its application aims to increase the tribological performance of such coatings. In this work were produced thin films of Si_3N_4 matrix where the MoS_2 is incorporated in varying amounts during the deposition process.

Results

The films were deposited in layers of about 10 nm (Si_3N_4) interspersed with variable MoS_2 quantities corresponding to the deposition times of 0, 0.3, 0.5, 0.7 and 1 s. Molybdenum disulfide and Si targets were used to produce the samples.

Samples were characterized by means of the Rutherford Backscattering technique. The backscattering spectrum for the film of Si_3N_4 with their characteristic peaks can be seen in Figure 1a. The calculated deposition rate for the film of Si_3N_4 is 0.12 nm/s as shown in Figure 1b. The stoichiometry of the compounds was found to be 0.74 for the Si/N atomic ratio and 0.5 for the Mo/S atomic ratio. The amount of MoS_2 in relation to the deposition time is shown in Figure 1c.

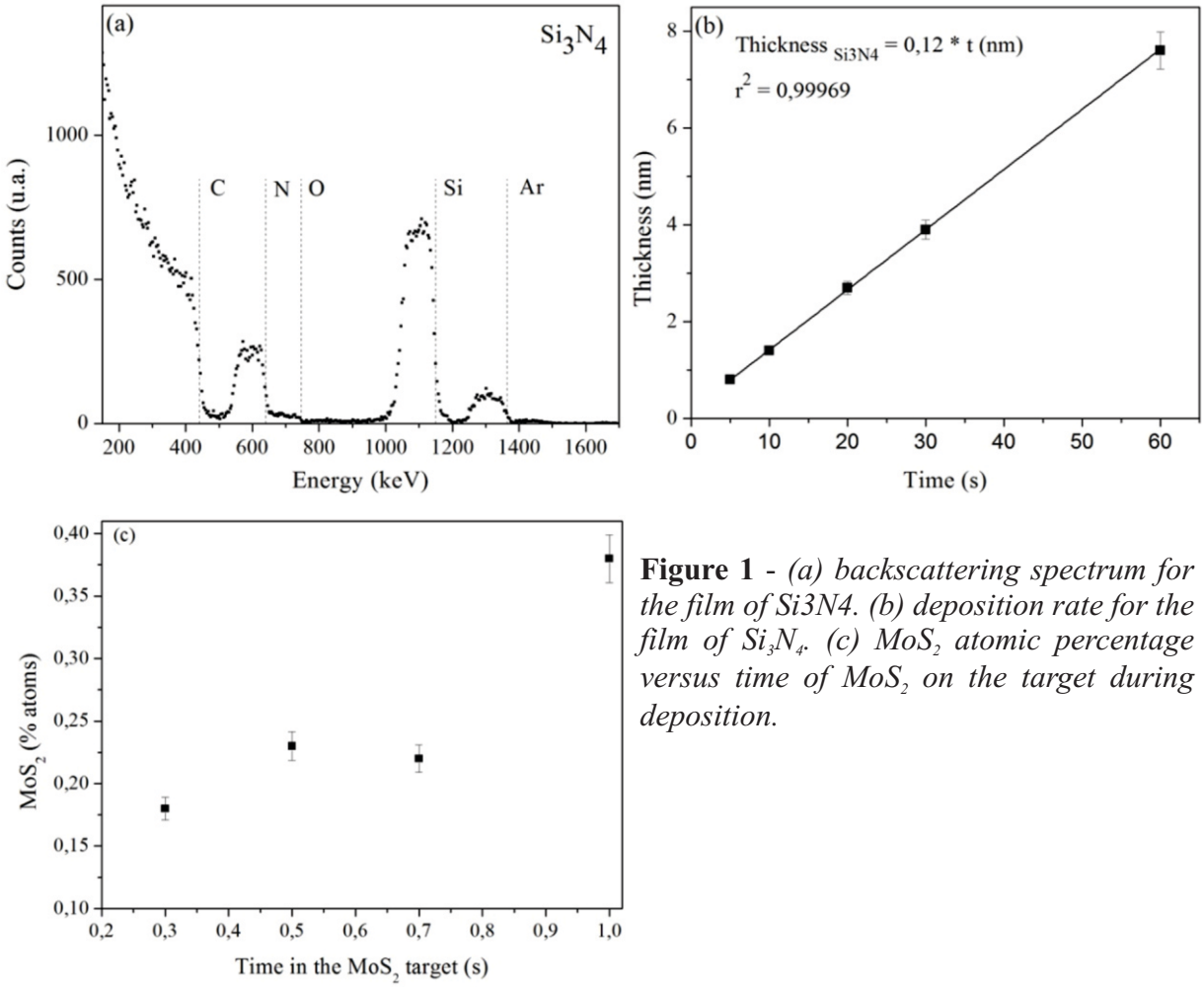

Figure 1 - *(a) backscattering spectrum for the film of Si3N4. (b) deposition rate for the film of Si_3N_4. (c) MoS_2 atomic percentage versus time of MoS_2 on the target during deposition.*

Research Outlook

In summary, it was demonstrated the possibility of co-deposition of materials (Si_3N_4 and MoS_2) and the formation of a stoichiometric film. These results allow the use of the reactive magnetron sputtering technique for the manufacture of films, and the evaluation of their mechanical and tribological properties, thus leading to the possibility of developing a functional compound.

Publications

[1] A.L. Bandeira; R. Trentin; C. Aguzzoli; M.E.H. Maia da Costa; A.F. Michels; I.J.R. Baumvol; M.C.M. Farias, C.A. Figueroa, *Sliding Wear and Friction Behavior of CrN-coating in Ethanol and Oil-Ethanol Mixture*, Wear, Submitted, (2012).

Lattent ion tracks in a-Ge

R. Giulian

Introduction

Ion-solid interactions during swift heavy-ion irradiation (SHII) are dominated by inelastic processes (electronic stopping) resulting in the excitation and ionisation of substrate atoms while, in contrast, the elastic processes (nuclear stopping) that lead to ballistic atomic displacements at much lower energies are negligible in the SHII regime. The energy dissipation in and amorphous material is usually confined to a smaller volume (when compared to its crystalline counterpart), as a result of a reduced electron mean free path and/or thermal conductivity. When the lattice temperature exceeds that required for substrate melting, a narrow cylinder of molten material is formed along the ion path and the ensuing rapid re-solidification of this transient liquid phase can yield remnant disorder within the substrate in the form of a latent ion track.

Results

We identify and characterise latent ion tracks formed in amorphous Ge by swift heavy-ion irradiation (185 MeV Au^{+13}), utilising experiment, first-principle calculations and simulations. For our irradiation conditions, tracks were formed only in amorphous material, as attributed to a much weaker electron-phonon coupling constant in crystalline material. Small-angle x-ray scattering measurements show the ion track structure is comprised of an under-dense core and over-dense shell that results from a quenched-in pressure wave emanating radially outwards following a thermal spike. Molecular Dynamics simulations indicate a solid-to-liquid phase transformation is operative within the ion track and the ensuing volume contraction necessary to accommodate the high-density molten phase produces open volume in the form of voids interspersed along the ion path.

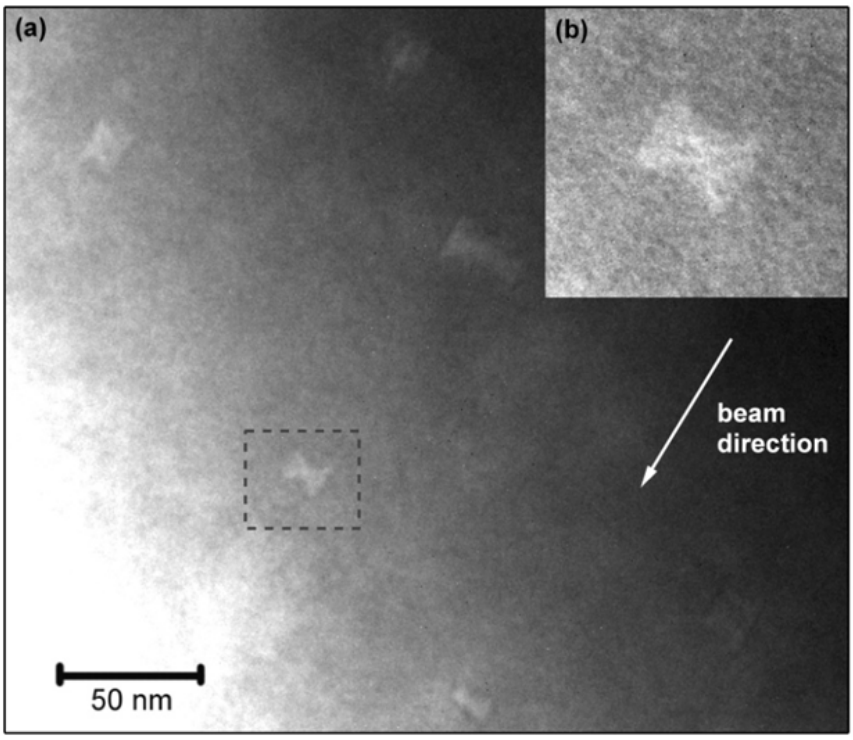

Figure 1 - *(a) XTEM image recorded at a depth of 1 μm in a-Ge irradiated with 185 MeV Au ions to a fluence of* $6x10^{10}$ */cm*^{2} *. (b) Magnified view of the selected area.*

The voids are of bow-tie-like shape and aligned with the incident ion direction. Their unique geometry, as imaged with transmission electron microscopy, is reproduced with simulation and shown to result from a radially inward re-solidification. We suggest these voids are the precursor to the widely-reported swift heavy-ion irradiation-induced porosity in amorphous Ge. Experiment and simulation are well correlated and now provide unambiguous evidence of ion track formation in an amorphous semiconductor.

Research Outlook

This study will be extended to include other materials, like GaSb, InSb and AlSb.

Publications

[1] M.C. Ridgway, T. Bierschenk, R.Giulian, B. Afra, M.D. Rodriguez, L.L. Araujo, A.P. Byrne,N. Kirby, O.H. Pakarinen, F. Djurabekova, K. Nordlund, M. Schleberger, O. Osmani, N. Medvedev, B. Rethfeld,W. Wesch and P. Kluth, *Lattent ion tracks in amorphous Ge*, Physical Review Letters, in press (2012)

Electronic stopping cross sections for protons in Al_2O_3

R. C. Fadanelli

Introduction

Alumina (Al_2O_3) is an important material broadly used in mechanical, optical, optoelectronics or microelectronic applications due to its excellent chemical resistance, good mechanical strength, high hardness, transparency, high abrasion and corrosion resistance. On the other hand, the study of the energy deposition of energetic ions in matter is a problem of interest for basic and applied research in many areas. A significant dispersion among the previous H experimental stopping data has been an incentive to carry out new H stopping measurements in a Al_2O_3 matrix covering a broad range of energies. Thus, our work consists in an experimental-theoretical study of the stopping power of Al_2O_3 for proton beams. With this purpose we have measured the stopping cross section (SCS) in an energy interval going from 40 keV up to 1 MeV by using two different techniques: Rutherford backscattering spectrometry (RBS) and the transmission method. Theoretical calculations of the SCS are based on the linear dielectric formalism (GOS) and on the nonlinear transport-cross-section model (TCS).

Results

In Figure 1 are shown the present and previous experimental results of the H stopping power into Al_2O_3 target together with the predictions of the theoretical models. The total SCS of Al_2O_3 for protons was obtained as the sum of two contributions: (i) the contribution of valence electrons, calculated with the TCS formalism; and (ii) the inner-shell contribution, obtained using the GOS method. We find that these calculations are in a quite satisfactory agreement with our experimental data on the whole range of energies considered, including the maximum of the stopping power.

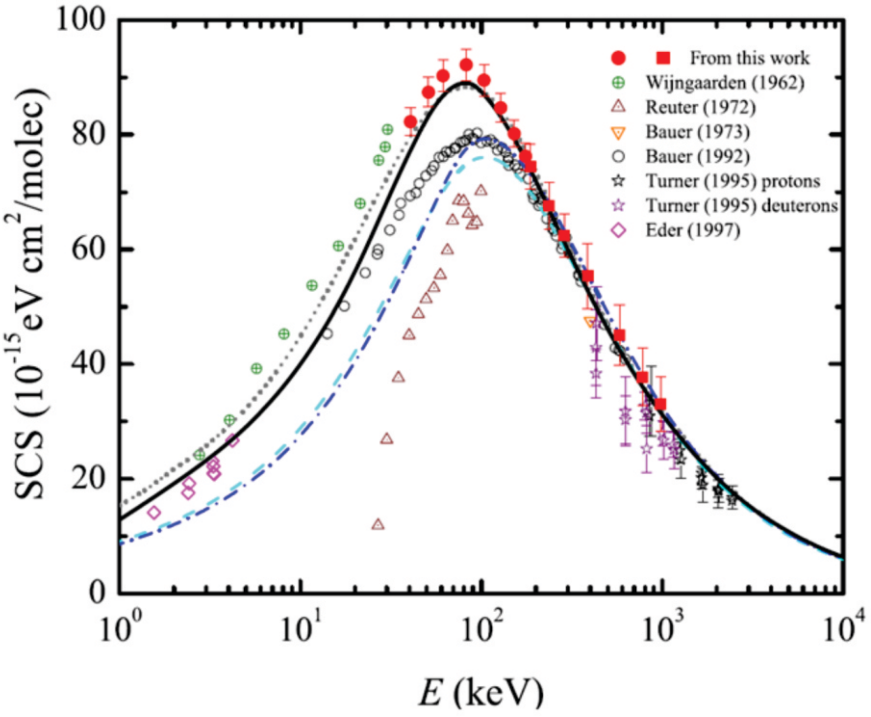

Figure 1 - *Stopping cross section (SCS) of Al_2O_3 measured for a proton beam as a function of the incident energy are represented by red symbols. Other symbols correspond to experimental data available in the literature. Black solid line corresponds to the SCS from the non-lineal TCS model together with the GOS model. Blue dash-dotted line and cyan dashed line are the results from the dielectric formalism with the MELF-GOS. The result obtained by the semiempirical SRIM code is depicted by a grey dotted line.*

Research Outlook

The theoretical-experimental procedure carried on in this work can be used to study the SCS of H and He in other oxides, namely TiO_2 and TaO_2. Both oxides are important from a technical viewpoint.

Publications

[1] M. Behar, R. C. Fadanelli, L. C. C. M. Nagamine, E. D. Cantero, G. H. Lantschner, J. C. Eckardt, N. R. Arista, R. García-Molina, and I. Abril. *Electronic stopping cross sections for protons in Al_2O_3 : an experimental and theoretical study*. The European Physical Journal D, **66**, 247 (2012).
[2] E. D. Cantero, R. C. Fadanelli, M. Behar, L. C. C. M. Nagamine, G. H Lantschner, and J. C. Eckardt. *Experimental study of the He stopping power into Al_2O_3 films*. Nuclear Instruments and Methods in Physics Research B. **B287**, 1 (2012).

Determination of film thicknesses through the breakup of H_2^+ ions

S. M. Shubeita, R. C. Fadanelli, J. F. Dias, and P. L. Grande

Introduction

Depth profiling heavy elements in thin films is a requirement in the modern materials science. Ion scattering techniques express depth in units of length assuming the knowledge of the density of the target otherwise "depth" stands as an abbreviation for the number of atoms per unit area. Therefore, a method to determine the absolute depth without the knowledge of the density is useful.

We explore a new method to determine absolute thicknesses of ultra-thin amorphous films, based on the measurement of the dwell time of hydrogen fragments traversing amorphous films under the quasi-Coulomb explosion (Figure 1). High energy-resolution backscattering experiments were performed with incident H^+ and H_2^+ ions interacting with ultra-thin films like LaAlO3, HfO_2 and $LaScO_3$.

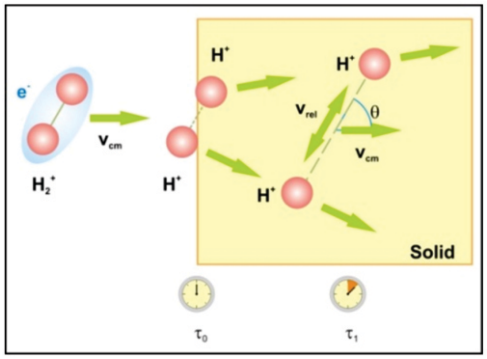

Figure 1 - *Schematic drawing depicting the concept behind the Coulomb explosion profiling technique. As soon as the H_2^+ molecule penetrates the target, it loses its electron and the Coulomb explosion pushes the H^+ fragments away from each other with a relative velocity v_{rel}.*

Results

Figure 2(a) shows the experimental results obtained for the Coulomb broadening c(x) when 150 keV/nucleon H_2^+ ions interacting with HfO_2 and $LaScO_3$ films are considered. Calculations using pure Coulomb and Yukawa repulsive potentials are shown as well. The experimental results are in good agreement with the calculations considering a screened repulsive potential for both targets and indicate that the densities employed in the calculations of both films correspond to the actual densities (ρ= 9.7 g/cm^3 for HfO_2 and ρ = 4.04 g/cm^3 for $LaScO_3$). The Coulomb broadening for 150 keV/nucleon H_2^+ ions interacting with the $LaAlO_3$ target are displayed in Figure 2(b) and show

The values of c(x) (blue squares) are much larger than those obtained from the calculations using a screened Yukawa potential (red line), and even larger than those obtained from a pure Coulomb potential (black line).

Therefore, the disagreement between experiment (blue squares) and theory (red line) indicates that the thickness obtained for the proton case is not compatible with the increment on the energy-loss straggling promoted by the H_2^+ ions. In order to provide more "time" to the explosion, the actual thickness of the film has to be larger. This implies a reduced value for the density since the product of thickness and density is fixed by the standard experiment with protons. The best density can be found simply by stretching the x scale, leading to a value of 3.9 g/cm^3. This result is corroborated by TEM image of the film (inset of Fig. 2(b)).

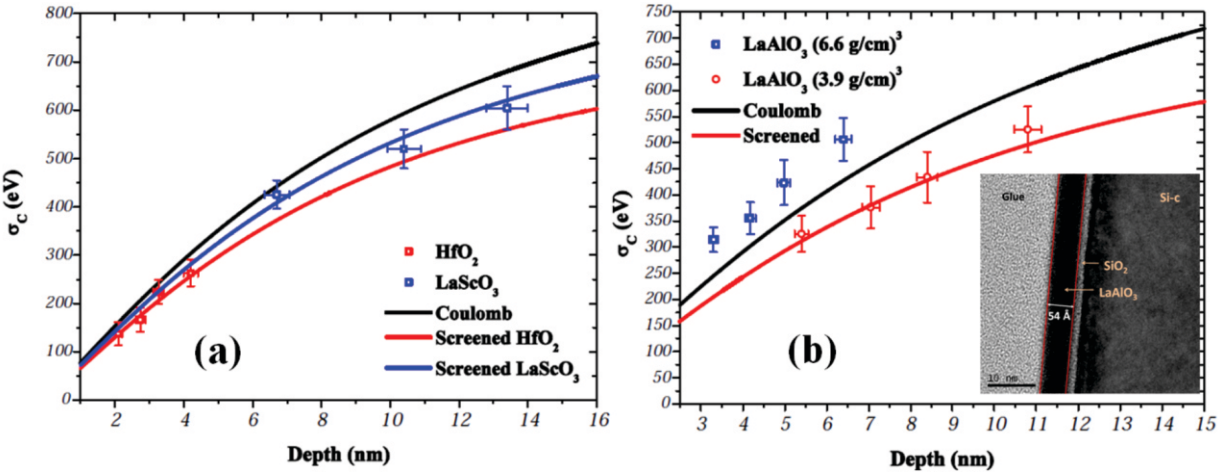

Figure 2 - *(a) The Coulomb broadening as a function of the depth traversed by the molecular fragments of H_2^+ molecules in ultra-thin $LaScO_3$ (blue squares) and HfO_2 (red squares) films. The curves represent the calculations of Coulomb broadening assuming a pure Coulomb repulsive potential (black line) and a screened repulsive potential for $LaScO_3$ (blue line) and HfO_2 (red line). (b) The same as in (a) for $LaAlO_3$ film. Blue squares and red circles stand for experimental results assuming a density of ρ= 6.6 g/cm^3 and ρ= 3.9 g/cm^3 respectively. The inset shows the TEM results of the film under consideration.*

Research Outlook

Our results show that the study of the Coulomb explosion and the dwell time of 150 keV/nucleon H_2^+ molecules traversing ultra-thin films constitute a powerful technique to determine absolute thicknesses and densities of amorphous targets. Further theoretical investigations on the polarization field and corresponding effective interaction of ion clusters inside the matter are needed in order to improve the applicability of the proposed technique.

Publications

[1] S. M. Shubeita, R. C. Fadanelli, J. F. Dias, P. L. Grande, *Determination of film thicknesses through the breakup of H_2^+ ions*, Surface Science, In press (2012).

Tailoring HC of unbiased FM/AF bilayers

K. D. Sossmeier, D. Schafer, J. E. Schmidt, J. Geshev

Introduction

Systems composed of a ferromagnet (FM) exchange-coupled to an antiferromagnet (AF) present exchange bias (EB), i.e., a shift of the magnetization curve along the magnetic field axis, accompanied by an increase of the coercivity (HC). In EB systems, both EB field magnitude and EB direction can be modified through ion bombardment in the presence of magnetic field. Here we present results on an unconventional magnetron-sputtered system which does not present EB at room temperature. Pieces of the as-made IrMn/NiCu bilayer and of a NiCu single layer were irradiated with He, Ar or Ge ions at different fluences or annealed at different temperatures (TANN). The unconventionality of our exchange-coupled FM/AF system refers to the fact that the Curie temperature (TC) of the FM layer is rather lower than the Néel temperature (TN) of the IrMn AF layer.

Results

Due to the exchange coupling at the FM/AF interface, HC of the as-deposited FM/AF bilayer is rather higher than that of the corresponding FM single layer. We found that by choosing a proper ion fluence or annealing temperature, it is possible to controllably vary HC. Ion irradiation of the FM single layer has lead to only a decrease of HC and annealing or He ion irradiation has not caused important changes at the FM/AF interface; nevertheless, a twofold increase of HC was obtained after these treatments. Even more significant enhancement of HC was attained after Ge ion irradiation and attributed to ion-implantation-induced modification of only the FM layer; damages of the FM/AF interface, on the other hand, decrease the coercivity.

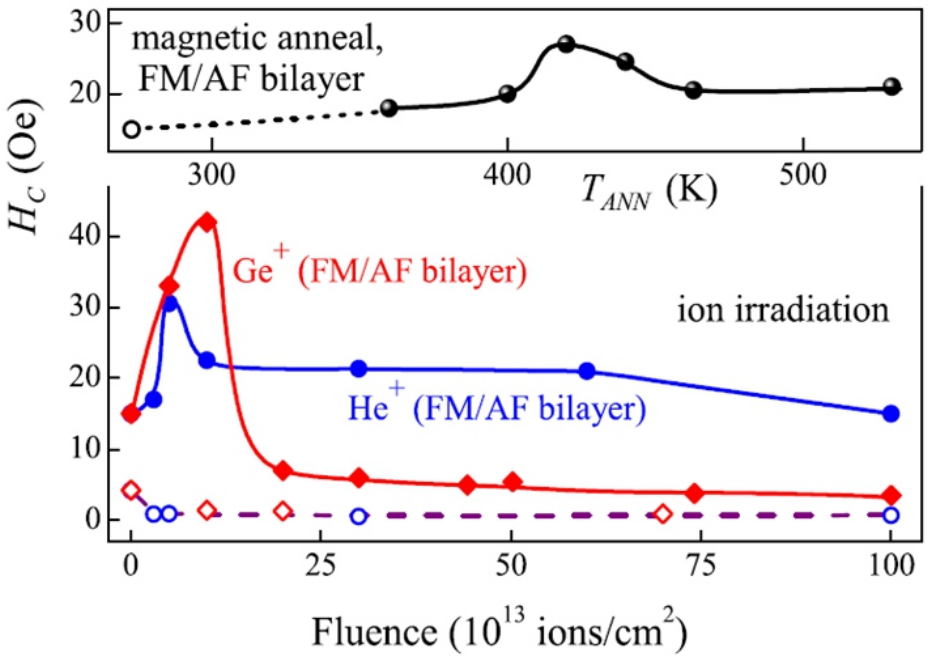

Figure 1 - *Variations of HC of the FM/AF bilayer with the annealing temperature (top) and with the fluence for the cases of He^+ or Ge^+ irradiation (bottom). The empty circles and diamonds represent the respective HC data of the FM single layer obtained after He^+ or Ge^+ irradiations, respectively. The error in HC is twice the size of the symbols and the lines are guides to the eyes.*

Research Outlook

Ion irradiation/implantation has been shown to be a useful tool for modification of the structural and compositional properties of magnetic materials. Despite a number of very interesting effects related to FM/AF coupling observed in thin films and in AF nanoparticles with ferrimagnetic shells with TN higher or close to TC and regardless of their potential technological applicability, studies on such systems are still rather scarce owing to the difficulties in initializing and manipulating the EB effect. We showed that, by choosing adequate ion fluence or TANN, one can obtain a controlled variation of more than one order of magnitude of the coercivity of unconventional exchange-coupled though unbiased IrMn/ NiCu thin films.

Publications

[1] K. D. Sossmeier, D. Schafer, A. P. O. Bastos, J. E. Schmidt, and J. Geshev, *Tailoring coercivity of unbiased exchange-coupled FM/AF bilayers*, Journ. Appl. Phys., **112**, 013904 (2012)

A possible approach to analyze neurological processes in the brain

P. Jobim, C. E. I. dos Santos, N. Maurmann, T. R. Pedroso, G. k. Reolon, M. Blank, M. L. Yoneama, R. Debastiani, J. F. Dias

Introduction

Knowledge about the distribution and concentration of trace elements in tissues is of utmost importance since trace elements are related with several biological functions. Zn, Ca, K, Na, Cl, Cu, S, Al and P may play a role in brain concerning memory formation and learning. Among some methods to measure the elemental distribution in animal brain, PIXE and microprobe techniques could be very useful to achieve this goal. The aim of this work is to develop a sample preparation protocol for ion beam techniques analysis and investigate the elemental composition and distribution during the memory formation process [1,2].

Results

PIXE results showed that PIXE spectra of brain consist of Mg, Al, P, S, Cl, K, Ca, Fe, Cu, Zn and Rb. Moreover, the memory acquisition process is characterized by increased synthesis of Ca, Mg Fe and Zn (Figure 1). Therefore, the alterations in the elemental concentrations may indicate their participation in the memory formation (learning) and accessibility (reminder).

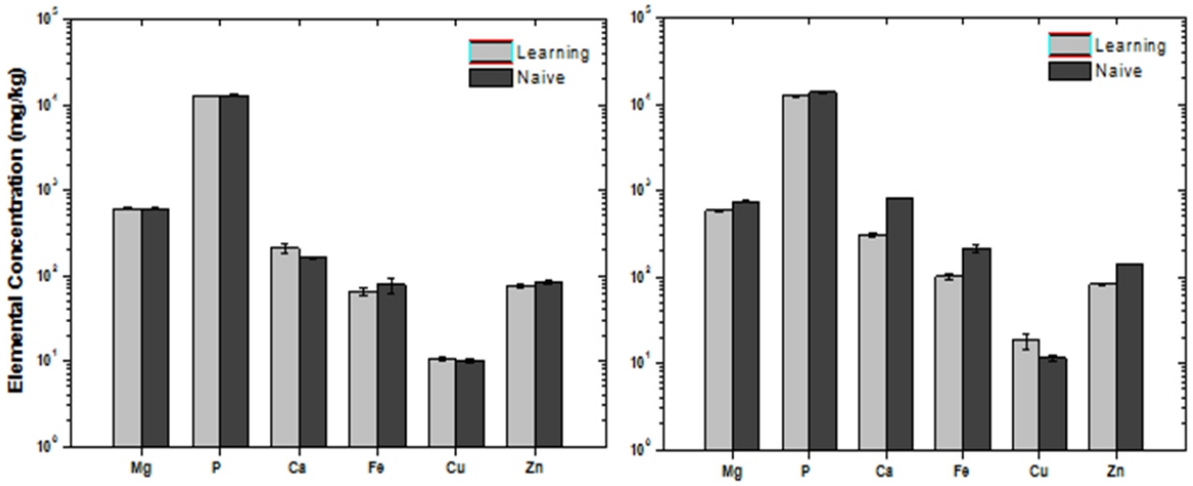

Figure 1 - *PIXE analyzes comparing animal hippocampus (left) and cortex (right). Group "learning" in gray represents the rats which pass through a single inhibition avoidance trial and were sacrificed 3 hours later, i. e., during the second wave of protein synthesis. Group "naïve" in black represent the rats that were not exposed to any apparent stimuli.*

Research Outlook

- Analysis of brain tissues;
- Analysis of otholits;
- Elemental composition of food;
- Proton beam writing of polymers;
- Analysis of gun shot residues.

Publications

[1] P. Jobim, T. Pedroso et al., *Impairment of object recognition memory by rapamycin inhibition of mTOR in the amygdala or hippocampus around the time of learning or reactivation*, Behavior Brain Research , **228**(1), 151 (2012)
[2] P. Jobim, T. Pedroso et al., *Inhibition of mTOR by rapamycin in the amygdala or hippocampus impairs formation and reconsolidation of inhibitory avoidance memory, Neurobiology of Learning and Memory*, **97**(1), 105(2012)

Open scientific software and instruments for Ion Beam Physics

M. Müller , J. Tambara , R. P. Pezzi

Introduction

We report on the development of open software and scientific instrumentation at the Ion Implantation Laboratory. With the objectives of 1) renew outdated instrumentation, 2) reduce our dependence on external closed technology and at the same time 3) preparing human resources capable of understanding and developing scientific instrumentation, our group is engaged in research and development of data acquisition and simulation software tools for ion beam physics. We highlight the Open Flatus and Spectrometry Station projects whose objectives are to perform ion energy loss simulations and spectroscopy data acquisition, respectively. Having adopted an open development approach in order to take advantage of collaborative and reproductive methodologies, our results are open to use, study, modification and distribution by anyone.

Results

Open Flatus: Simulates the energy loss processes in matter using stochastic energy loss models. Suitable for medium energy ion scattering spectra of amorphous targets. Implementation for Narrow Nuclear Resonance Profiling under way. It is implemented on the python programming language.

Spectrometry Station: Open source interface for the CAEN N957 multi channel analyzer. A code implemented in C acquires the data in real time while a python program is responsible for the graphics and user interface.

Both projects are available under the open licenses and can be found at http://cta.if.ufrgs.br/projects/open-flatus/ and http://cta.if.ufrgs.br/projects/estacao-de-espectrometria

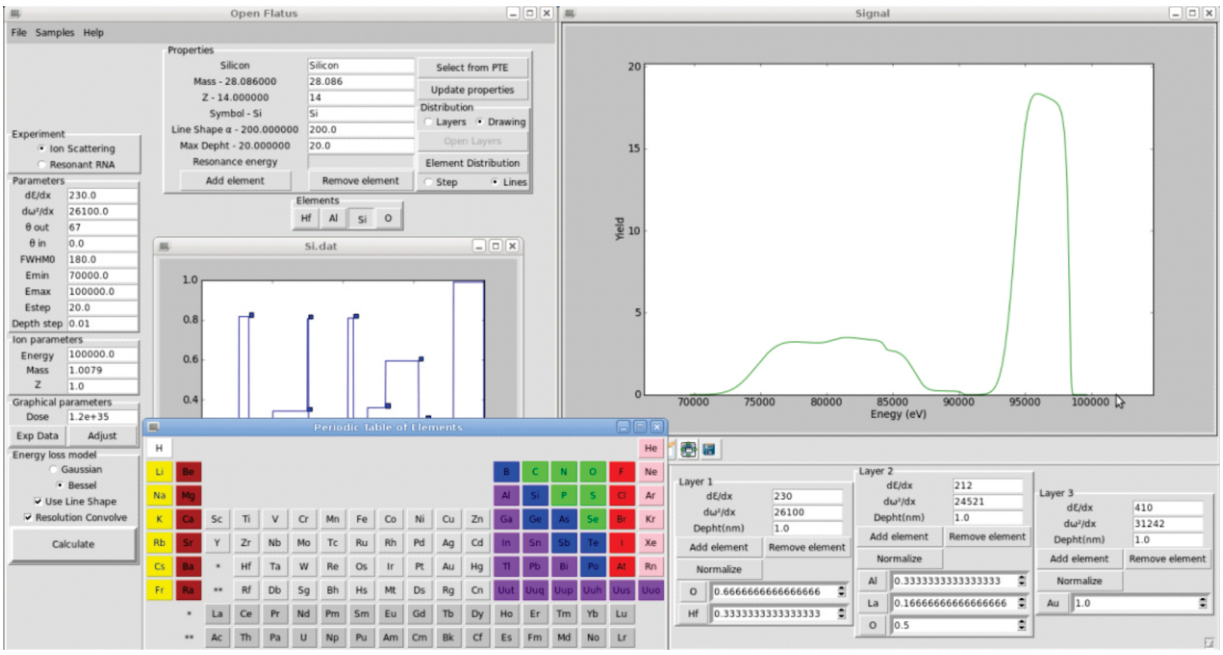

Figure 1 - *Open flatus: Medium Energy Ion Scattering Simulation of 100 keV H^+ ions on 5 nm Al-doped HfO_2 film on a Si substrate.*

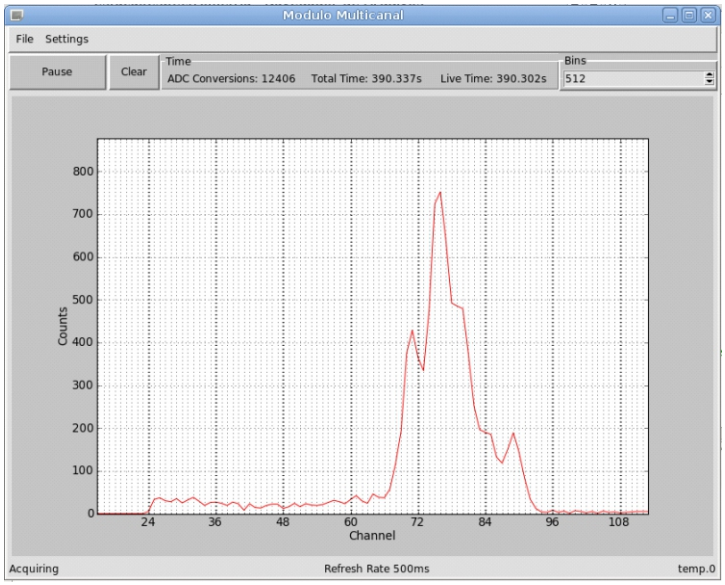

Figure 2 - *Main window of the spectrometry station showing real time PIXE spectrum acquisition corresponding to SnOx samples using CAEN N957 MCA. The peaks correspond to Sn K lines.*

Research Outlook

We have implemented open solutions for data acquisition and data analysis in order to renew outdated instrumentation at the Ion Implantation Laboratory and reduce our dependence on external closed technology. Prototypes for stepper motor controllers for MEIS sample positioning have also been assembled.

Publications in peer reviewed articles

1) S. M. Shubeita, P. L. Grande, J. F. Dias, R. Garcia-Molina, C. D. Denton and I. Abril. “Energy loss of swift H2+ and H3+ molecules in gols: Vicinage effects”. Physical Review B, 83 (2011) 245423.

2) C. M. Viau, T. N. Guecheva, J. M. Cardone, M. L. Yoneama, J. F. Dias, C. Pungartnik, M. Brendel, J. Saffi and J. A. P. Henriques. “The role of yeast low-affinity iron and zinc transport systems in stannous-induced toxicity”. FEBS Journal, 278 (2011) 430.

3) O. de Melo, S. larramendi, M. Behar, D.G. Trabada and M. Velez. “Zn nanosheet network formation by ZnTe oxidationn in humid argon atmosphere annealing”. Material Letters, 216 (2012) 123.

4) R. Mazzei, G. G. Bermudez, D. E. Camporotondi, C. Arbeitmab, M. F.del Grosso and M. Behar. “New membranes obtained by grafted irradiated PVDF foils”. Nuclear instruments and methods in physics research, section B, Beam interactions with materials and atoms, 287 (2012) 26.

5) N.M. Bom, G.V. Soares, C. Krug, R.P. Pezzi, I.J.R. Baumvol and C. Radtke. “Evolution of the Al2O3/Ge(100) interface for reactively sputter-deposited films submitted to postdeposition anneals”. Applied Surface Science, 258 (2012) 5707.

6) S. R. M. da Silva, G. K. Rolim, G. V. Soares, I. J. R. Baumvol, C. Krug, L. Miotti, F. L. Freire, M. E. H. M. da Costa and C. Radtke. “Oxygen transport and GeO2 stability during thermal oxidation of Ge”. Applied Physics Letters, 100 (2012) 191907.

7) S. A. Corrêa, G. V. Soares, C. Radtke and F. C. Stedile. “Unraveling the role of SiC or Si substrates in water vapor incorporation in SiO2 films thermally grown using ion beam analyses”. Nuclear instruments and methods in physics research, section B, Beam interactions with materials and atoms, 273 (2012) 139-141.

8) N. M. Bom, G. V. Soares, C. Krug, I. J. R. Baumvol and C. Radtke. “Probing the stability of Al2O3/Ge structures with ion beams”. Nuclear instruments and methods in physics research, section B, Beam interactions with materials and atoms, 273 (2012) 146.

9) F. Bonatto, S. Rovani, I. R. Kaufman, G.V. Soares, I. J. R. Baumvol and C. Krug. “Complementary low energy ion scattering and X-ray photoelectron spectroscopy characterization of polystyrene submitted to N-2/H-2 glow discharge”. Nuclear instruments and methods in physics research, section B, Beam interactions with materials and atoms, 273 (2012) 189.

10) F. L. Bregolin, U. S. Sias and M. Behar. “Photoluminescence and structural studies of Tb and Eu implanted at high temperatures into SiO2 films”. Journal of Luminescence, In Press, Corrected Proof. (Available online 15 October 2012).

11) E. D. Cantero, R. C. Fadanelli, M. Behar, L. C. C. M. Nagamine, G. H Lantschner, and J. C. Eckardt. “Experimental study of the He stopping power into Al2O3 films”. Nuclear instruments and methods in physics research, section B, Beam interactions with materials and atoms, 287 (2012) 1.

12) M. Behar, R. C. Fadanelli, L. C. C. M. Nagamine, E. D. Cantero, G. H. Lantschner, J. C. Eckardt, N. R. Arista, R. García-Molina, and I. Abril. “Electronic stopping cross sections for protons in Al2O3 : an experimental and theoretical study”. The european physical journal D, atomic, molecular, optical and plasma physics, 66 (2012) 247.

13) M. D. Rodríguez, B. Afra, C. Trautmann, M. Toulemonde, T. Bierschenk, J. Leslie, R. Giulian, N. Kirby and P. Kluth. “Morphology of swift heavy ion tracks in metallic glasses”. Journal of Non-Crystalline Solids, 358 (2012) 571.

14) L. L. Araujo, R. Giulian, D. J. Sprouster, C. S. Schnohr, D. J. Llewellyn, B. Johannessen, A. P. Byrne and M. C. Ridgway. “Structural properties of embedded Ge nanoparticles modified by swift heavy-ion irradiation”. Physical Review B, 85 (2012) 235417.

15) M. D. Rodríguez, C. Trautmann, M. Toulemonde, B. Afra, T. Bierschenk, R. Giulian, N. Kirby and P. Kluth. “Modification of Fe-B based metallic glasses using swift heavy ions”. EPJ Web of Conferences, 35 (2012) 03004.

16) P. Kluth, F. Djurabekova, K. Nordlund, M. C. Ridgway, R. Giulian, A. P. Byrne and O. H. Pakarinen. “Nanoscale density fluctuations in swift heavy ion irradiated amorphous SiO2”. Journal of Applied Physics, 110 (2011) 123520.

17) R. Palmieri, C. Radtke, H. Boudinov and E.F. da Silva. “Effect of H2O2 in passivation of n- and p-type 4H-SiC surfaces”. Physica Status Solidi. A, 209 (2012) 675.

18) P. S. Correa, E. L. da Silva, R. F. da Silva, C. Radtke, B. Moreno, E. Chinaro and C. F. Malfati. “Effect of decreasing platinum amount in Pt Sn Ni alloys supported on carbon as electrocatalysts for ethanol electrooxidation”. International Journal of Hydrogen Energy, 37 (2012) 9314.

19) A. J. Window, A. Hentz, D. C. Sheppard, G. S. Parkinson, D. P. Woodruff, W. Unterberger, T. C. Q. Noakes, P. Bailey, M. V. Ganduglia-Pirovano and J. Sauer. “The structure of epitaxial V2O3 films and their surfaces: A medium energy ion scattering study”. Surface Science, 606 (2012) 1716.

20) M. A. Sortica, P. L. Grande, C. Radtke, L. G. Almeida, R. Debastiani, J. F. Dias and A. Hentz. “Structural characterization of CdSe/ZnS quantum dots using medium energy ion scattering”. Applied Physics Letters, 101 (2012) 0231101.

21) C. Aguzzoli, C. A. Figueroa, F. S. de Souza, A. Spinelli and I. J. R. Baumvol. “Corrosion and nanomechanical properties of vanadium carbide thin film coatings of tool steel”. Surface & Coatings Technology, 206 (2012) 2725.

22) C. Luvison, V. Sonda, A. C. Rovani, F. Cemin, F. G. Echeverrigaray, C. Aguzzoli, A. E. Crespi, C. L. G. Amorim, M. E. H. Maia da Costa, I. J. R. Baumvol and C. A. Figueroa. “Friction in near surface regions of plain steel plasma-nitrided and post oxidized at various hydrogen contents”. Vacuum, 86 (2012) 1268.

23) M. S. Farias, P. Budni, C. M. Ribeiro, E. B. Parisotto, C. E. I. dos Santos, J. F. Dias, E. M. Dalmarco, T. S. Fröde, R. C. Pedrosa and D. Wilhelm Filho. “Antioxidant supplementation attenuates oxidative stress in chronic hepatitis C patients”. Gastroenterología y Hepatología, 35 (2012) 386.

24) F. R. da Silva, J. da Silva, M. C. Allgayer, C. F. Simon, J. F. Dias, C. E. I. dos Santos, M. Salvador, C. Branco, N. B. Schneider, V. Kahl, P. Rohr and K. Kvitko. “Genotoxic biomonitoring of tobacco farmers: Biomarkers of exposure, of early biological effects and of susceptibility”. Journal of Hazardous Materials, 225-226 (2012) 81.

25) P. Rohr, J. da Silva, F. R. da Silva, M. Sarmento, C. Porto, R. Debastiani, C. E. I. dos Santos, J. F. Dias and K. Kvitko. “Evaluation of genetic damage in open-cast coalmine workers using the buccal micronucleus cytome assay”. Environmental and MolecularMutagenesis, in press, (2012).

26) P. F. C. Jobim, T. R. Pedroso, A. Werenicz, R. R. Christoff, N. Maurmann, G. K. Reolon, N. Schröder and R. Roesler. “Impairment of object recognition memory by rapamycin inhibition of mTOR in the amygdala or hippocampus around the time of learning or reactivation”. Behavioural Brain Research, 228 (2012) 151.

27) A. Werenicz, R. R. Christoff, M. Blank, P. F. Jobim, T. R. Pedroso, G. K. Reolon, N. Schröder and R. Roesler. “Administration of the phosphodiesterase type 4 inhibitor rolipram into the amygdala at a specific time interval after learning increases recognition memory persistence”. Learning and Memory, 19 (2012) 495.

28) P. F. Jobim, T. R. Pedroso, R. R. Christoff, A. Werenicz, N. Maurmann, G. K. Reolon and R. Roesler. “Inhibition of mTOR by rapamycin in the amygdala or hippocampus impairs formation and reconsolidation of inhibitory avoidance memory”. Neurobilogy of Learning and Memory, 97(1) (2012) 105.

29) R. H. Garcia, M. Behar, J. F. Dias, M. E. V. Tagle, M. D. D. Rodriguez, F. P. C. Pinar and M. S. P. Alfonso. “Determination of Pb, Zr, Ti, Sr, Cr, Nb and La in lead zirconate titanate ceramics by particle-induced X-ray emission”. X-Ray Spectrometry, 41 (2012) 156.

30) C. Dani, L. S. Oliboni, D. Prá, D. Bonatto, C. E. I. dos Santos, M. L. Yoneama, J. F. Dias, M. Salvador and J. A. P. Henriques. “Mineral content is related to antioxidant and antimutagenic properties of grape juice”. Genetics and Molecular Research, 11(3) (2012) 3154.

31) M. S. Farias, P. Budni, C. M. Ribeiro, E. B. Parisotto, C. E. I. Santos, J. F. Dias, E. M. Dalmarco, T. S. Frode, R. C. Pedrosa and D. W. Filho. “Antioxidat supplementation attenuates oxidative stress in chronic hepatitis C patients”. Gastroenterología y Hepatolgía, 35 (2012) 386.

32) V. A. Barrera, J. Miranda, A. A. Espinosa, J. Melinguer, J. N. Martínez, E. Cerón, J. R. Morales, P. A. Miranda and J. F. Dias. “Contribution of soil, sulfate and biomass burning sources to the elemental composition of PM10 from Mexico City”. International Journal of Environmental Research, 6(3) (2012) 597.

33) V. M. Viau, J. M. Cardone, T. N. Guecheva, M. L. Yoneama, J. F. Dias, C. Pungartnik, M. Brendel, J. Saffi and J. A. P. Henriques. “Enhanced resistance of yeast mutants deficient in low-affinity iron and zinc transporters to stannous-induced toxicity”. Chemosphere, 88 (2012) 477.

34) R. O. Cunha, D. L. Baptista, M. Heinemann, M. F. Kuhn, J. E. Schmidt and L. G. Pereira. “Reference layer exchange in spin transfer torque experiment using magnetic-coated nanometric point contacts”. Journal of Magnetism and Magnetic Materials, 324 (2012) 3002.

35) A. Jorio, J. Ribeiro-Soares, L. G. Cançado, N. P. S. Falcão, H. F. Dos Santos, D. L. Baptista, E. H. Martins Ferreira, B. S. Archanjo and C. A. Achete. “Microscopy and spectroscopy analysis of carbon nanostructures in highly fertile Amazonian anthrosoils”. Soil & Tillage Research, 122 (2012) 61.

36) A. Lopez-Bezanilla, J. Campos-Delgado, G. Bobby, D. L. Baptista, T. Hayashi, Y. A. Kim, H. Muramatsu, M. Endo, C. A. Achete, M. Terrones and V. Meunier. “Geometric and Electronic Structure of Closed Graphene Edges”. Journal of Physical Chemistry Letters, 3 (2012) 2097.

37) J. Campos-Delgado, D. L. Baptista, M. F. Cabrera, B. G. Sumpter, V. Meunier, H. Terrones, Y. A. Kim, H. Muramatsu, T. Hayashi, M. Endo, M. Terrones and A. C. Achete. “Iron Particle Nanodrilling of Few Layer Graphene at Low Electron Beam Accelerating Voltages”. Particle & Particle Systems Characterization, 2012.

38) E. M. Stori, C. T. de Souza, D. Fink, R. M. Papaléo, L. Amaral and J. F. Dias. “Use of STIM for Morphological Studies of Microstructured Polymer Foils”. Nuclear Instruments and Methods in Physics Research Section B: Beam Interactions with Materials and Atoms, (2013) in press.

39) R. M. S. dos Reis, R. L. Maltez, E. C. Moreira, Y. P. Dias and H. Boudinov. “Raman and TEM characterization of high fluence C implanted nanometric Si on insulator”. Applied Surface Science, 255 (2012) 7395.

40) G. Schiwietz and P. L. Grande. “Stopping of Protons – Improved accuracy of the UCA model”. Nuclear Instruments and Methods in Physics Research Section B: Beam Interactions with Materials and Atoms, 273 (2012) 1–5.

41) J. Leveneur, D. F. Sanchez, J. Kennedy, P. L. Grande, G. V. M. Williams, J. B. Metson and B. C. C. Cowie. “Iron-based bimagnetic core/shell nanostructures in SiO2: a TEM, MEIS, and energy-resolved XPS analysis”. Journal of Nanoparticles Research, 14 (2012) 1149.

42) A. L'Hoir, C. Cohen, J. J. Ganem, I. Trimaille, I. C. Vickridge and S. M. Shubeita. “Vicinage effect for hydrogen clusters in Si3N4 and SiO2”. Physical Review A, 85 (2012) 042901.

43) S. M. Shubeita, R. C. Fadanelli, J. F. Dias and P. L. Grande. "Determination of film thicknesses through the breakup of H2+ ions". Surface Science, (2012) in press.

44) A. Gasperini, A. Malachias, G. Fabbris, G. Kellermann, A. Gobbi, E. Avendaño and G. de M. Azevedo. "Investigation of indirect structural and chemical parameters of GeSi nanoparticles in a silica matrix by combined synchrotron radiation techniques". Journal of Applied Crystallography, 45 (2012) 71.

45) S. Nicolodi, L. Pereira, A. Harres, G. de M. Azevedo, J. Schmidt,I. García-Aguilar, N. Souza-Neto, C . Deranlot, C. F. Petroff and J. Geshev. "Negative rotatable anisotropy in IrMn/Cr/Co thin films". Physical Review B, 85 (2012) 224438.

46) E. Bittar, C. Adriano, T. Garitezi, P. Rosa, L. Mendonça-Ferreira, F. Garcia, G. de M. Azevedo, P. Pagliuso and E. Granado. "Co-Substitution Effects on the Fe Valence in the BaFe2As2 Superconducting Compound: A Study of Hard X-Ray Absorption Spectroscopy". Physical Review Letters 107 (2011) 267402.

47) J. A. Gomes, G. de M. Azevedo, J. Depeyrot, J. Mestnik-Filho, F. L. O. Paula, F. Tourinho and R. Perzynsky. "Structural, Chemical and Magnetic Investigations of Core-Shell Zinc Ferrite Nanoparticles". Journal of Physical Chemistry C, online at dx.doi.org/10.1021/jp3055069 (2012).

48) E. Pitthan, R. Palmieri, S. A. Corrêa, G.V. Soares, H. I. Boudinov and F. C. Stedile. "The role played in the improvement of the SiO2/SiC interface by a thin SiO2 film thermally grown prior to oxide film deposition". ECS Solid-State Letters, 2 (2013) 8.

49) F. Kremer, F. P. Luce, Z. E. Fabrim, D. F. Sanchez, R. Lang, F. C. Zawislak and P. F. P. Fichtner. "Tailoring the blue-violet photoluminescence from Sn-implanted SiO2 using a two-step annealing process". Journal of Physics D-Applied Physics, 45 (2012) 095304.

50) V. Fernandes, I. L. Graff, J. Varalda, L. Amaral, P. F. P. Fichtner, D. Demaille, Y. Zheng, W. H. Schreiner and D. H. Mosca. "Valence evaluation of Cerium in nanocrystalline CeO2 films electrodeposited on Si substrates". Journal of the Electrochemical Society, 159 (2012) K-27.

Oral contributions and invited talks

1) Moni Behar: Fifth International Conference of Radiation Effects on the Matter, Kona, USA (2012). Invited talk.

2) Moni Behar: Conference on Ion Beam Modifications of Materials, Quindong, China, (2012). Oral presentation.

3) Gabriel Vieira Soares: 222nd Meeting of ECS — The Electrochemical Society. Honolulu, EUA, (2012). Oral presentation.

4) Cláudio Radtke: 221st Meeting of ECS — The Electrochemical Society. Seattle, EUA, (2012). Oral presentation.

5) Agenor Hentz: CAARI 2012 - 22nd International Conference on the Application of Accelerators in Research and Industry, Fort Worth, USA, Invited Talk.

6) Paulo Jobim: BIOPIXE 2011 - 7th Symposium on BIOPIXE, Sendai, Japan, Nov/2011. Oral presentation.

7) Carla E. I. dos Santos: BIOPIXE 2011 - 7th Symposium on BIOPIXE, Sendai, Japan, Nov/2011. Oral presentation.

8) Pedro Luis Grande : CAARI 2012 - 22nd International Conference on the Application of Accelerators in Research and Industry, Aug/2012 Fort Worth, USA, Invited Talk.

9) Pedro Luis Grande : ICACS 25 - 25th Conference on Atomic Collisions in Solids, Oct/2012, Kyoto, Japan. Oral Presentation.

10) Eduardo Pitthan : XI Brazilian Materials Research Society Meeting, Sep/2012, Florianópolis, Brazil. Oral Presentation.

11) Silma Alberton Corrêa: XI Brazilian Materials Research Society Meeting, Sep/2012, Florianópolis, Brazil. Oral Presentation.

12)Silma Alberton Corrêa: 9th ECSCRM - The 9th European Conference on Silicon Carbide and Related Materials, Sep/2012, Saint Petersburg, Russia. Oral Presentation.

13)Silma Alberton Corrêa: 2012 Materials Research Society Spring Meeting & Exhibit, Apr/2012, San Francisco, USA. Oral Presentation.

Books and book chapters

1) R. C. Fadanelli, M. Behar, and J. F. Dias. "Coulomb heating behaviour of fast light diclusters in Si<100> direction". In: Ion implantation. Rijeka: In Tech, (2012) 47-62.

2) M. Sortica; D. Sanchez; P.L Grande; Engenharia de Superfícies; e-book; ISBN 978-85-66176-00-1.

3) F.C. Stedile, C. Radtke, G.V. Soares, E. Pitthan, R. Palmieri, S.A. Corrêa, “SiO2/SiC Interfacial Region: Presence of Silicon Oxycarbides and Effects of Hydrogen Peroxide and Water Vapor Thermal Treatments”, in Materials Science Forum, vol. 717-720, págs. 747-752, Trans Tech Publications, Suíça, 2012.

4) E. Pitthan, S.A. Corrêa, R. Palmieri, G.V. Soares, H.I. Boudinov, F.C. Stedile, “Improvement in the SiO2/4H-SiC interfacial region by thermal treatments with hydrogen peroxide”, in Materials Science Forum, vol. 717-720, págs. 753-756, Trans Tech Publications, Suíça, 2012.

Theses and Dissertations

1) Felipe L. Bregolin. Phd Thesis (2012).
Supervisor: Moni Behar. Co-supervisor: Uilson S. Sias.

2) Flavia P. Luce, PhD Thesis (2012).
Supervisor: Paulo F. P. Fichtner. Co-supervisor: Fernando C. Zawislak.

3) Aline Tais da Rosa, MSc Dissertation (2012).
Supervisor: Fernanda C. Stedile

4) André L. F. Cauduro, MSc Dissertation (2012).
Supervisor: Daniel L. Baptista.

5) Guilherme Sombrio. MSc Dissertation (2012).
Supervisor: H. Boudinov.

6) Ludmar G. Matos, MSc Dissertation (2012).
Supervisor: Rogerio L. Maltez.

7) Rafela Debastiani, MSc Dissertation (2012).
Supervisor: J. F. Dias.

Members in international commitees and in editorial boards of scientific journals

• Fernanda C. Stedile - Member of the international committee of the International Conference on Ion Beam Analysis (IBA)
• Pedro L. Grande - Member of the international committee of the International Conference on Ion Beam Analysis (IBA)
• Pedro L. Grande - Member of the international committee of the International Conference of Atomic Collision in Solids (ICACS)
• Pedro L. Grande - Member of the international committee of the International Workshop on High-Resolution Depth Profiling (HRDP)
• Pedro L. Grande - Member of the International Committee of Colisiones Inelasticas na Materia
• Pedro L. Grande - Editorial Board Nucl. Instrum. and Methods B
• Fernanda C. Stedile - Editorial Board Nucl. Instrum. and Methods B
• Johnny Ferraz Dias - Member of the International Committee of the International Conference on Particle-Induced X-ray Emission
• Johnny Ferraz Dias - Member of the International Committee of the International Symposium on BioPIXE
• Moni Behar - Member of the International Committee of the Radiation Effects in Insulators.
• Moni Behar - Member of International Committee of Radiation Effects on the Materials.
• Moni Behar - Member of the International Committee of Colisiones Inelasticas na Materia
• Ricardo Papaléo - Member of the International Committee International Symposium on Swift Heavy Ions in Matter
• Gustavo Azevedo - Member of the Executive Committee of the IXAS (International XAFS Society)
• Paulo F. P. Fichtner - Member of the International Comittee of the Ion Beam Modification of Materials Conference.

Partners/Projects (Universities, Research Institutes and Companies)

PRONEX

INCT-INES

Nanobiotec

INCT-Namitec

PNPD-CAPES

R-NANO

PETROBRAS

École Polytechnique de Nancy, CAPES – Brafitec.

PUC - RJ, INCT e PROCAD.

UFSC

UFPR

CBPF

UFRJ

INMETRO.

Funding Agencies

CNPq
Conselho Nacional de Desenvolvimento Científico e Tecnológico

CAPES

inct NAMITEC

Instituto Nacional de Engenharia de Superfícies

BR PETROBRAS
Petróleo Brasileiro S.A.

Fapergs

PRONEX

Laboratório de Implantação Iônica
Instituto de Física
Universidade Federal do Rio Grande do Sul UFRGS

Av. Bento Gonçalves, 9500
91501 – 970 Porto Alegre, RS, Brazil
Phone: +55-51-3308-7004, Fax: +55-51-3308-7296
http://implantador.if.ufrgs.br

Laboratório de Implantação Iônica

Laboratório de Implantação
Instituto de Física - UFRGS
Porto Alegre
Brazil